Acta Pharmaceutica Sinica B 2025;15(1):314−330

Chinese Pharmaceutical Association
Institute of Materia Medica, Chinese Academy of Medical Sciences

Acta Pharmaceutica Sinica B

www.elsevier.com/locate/apsb
www.sciencedirect.com

ORIGINAL ARTICLE

Cerebral endothelial 3-mercaptopyruvate sulfurtransferase improves ischemia-induced cognitive impairment *via* interacting with protein phosphatase 2A

Li Zhu[a,b,†], Yi Huang[d,†], Jing Jin[e], Rongjun Zou[f], Rui Zuo[a], Yong Luo[a,b], Ziqing Song[a], Linfeng Dai[a], Minyi Zhang[a], Qiuhe Chen[a], Yunting Wang[g], Wei Wang[a,b,*], Rongrong He[c,*], Yang Chen[a,b,*]

[a]*School of Pharmaceutics, Guangzhou University of Chinese Medicine, Guangzhou Higher Education Mega Center, Guangzhou 510000, China*
[b]*State Key Laboratory of syndrome of Chinese medicine, Guangzhou University of Chinese Medicine, Guangzhou 510000, China*
[c]*Guangdong Engineering Research Center of Chinese Medicine & Disease Susceptibility, Jinan University, Guangzhou 510632, China*
[d]*Department of Stomatology, the First Affiliated Hospital, the School of Dental Medicine, Jinan University, Guangzhou 510632, China*
[e]*Institute of Materia Medica, Chinese Academy of Medical Sciences and Peking Union Medical College, Beijing 100700, China*
[f]*The Second Affiliated Hospital of Guangzhou University of Chinese Medicine, Guangzhou 510000, China*
[g]*Department of Pharmacological and Pharmaceutical Sciences, College of Pharmacy, University of Houston, Houston, TX 77204-5037, USA*

Received 26 March 2024; received in revised form 26 June 2024; accepted 25 July 2024

KEY WORDS

Cerebral endothelium;
Protein phosphatase 2A;
3-Mercaptopyruvate

Abstract The catalytic activity of 3-mercaptopyruvate (3MP) sulfurtransferase (MPST) converts 3MP to hydrogen sulfide (H_2S). However, the regulatory mechanisms governing MPST and its impact on the brain remain largely unexplored. Our study reveals the neuroprotective role of endothelial MPST-generated H_2S, regulated by protein phosphatase 2A (PP2A). Bioinformatics analysis and RNA sequencing demonstrated that endothelial PP2A is associated with neurodegenerative disease pathways.

*Corresponding authors.
E-mail addresses: ychen8@gzucm.edu.cn (Yang Chen), rongronghe@jnu.edu.cn (Rongrong He), wangwei26960@126.com (Wei Wang).
[†]These authors made equal contributions to this work.

Peer review under the responsibility of Chinese Pharmaceutical Association and Institute of Materia Medica, Chinese Academy of Medical Sciences.

https://doi.org/10.1016/j.apsb.2024.11.015

sulfurtransferase;
Hydrogen sulfide;
Calpain2;
Neuron;
Cognition

Cerebral ischemic mice exhibited significant inactivation of endothelial PP2A, evidenced by the reduction of PP2Acα in the brain endothelium. Mice with endothelium-specific null PP2A ($PP2A^{EC\text{-}cKO}$) exhibited neuronal loss, cognitive dysfunction, and long-term potentiation deficits. Postnatal inactivation of endothelial PP2A also contributes to cognitive dysfunction and neuronal loss. However, regaining endothelial PP2A activity by overexpressing *Ppp2ca* rescued neuronal dysfunction. Mechanistically, PP2A deficiency is intricately linked to the MPST−H_2S signaling pathway. A robust reduction in endothelial MPST-dependent H_2S production followed PP2A deficiency. Exogenous H_2S treatment and AAV-mediated overexpression of MPST in brain endothelial cells significantly mitigated neuronal dysfunction in $PP2A^{EC\text{-}cKO}$ mice. Furthermore, PP2A deficiency promotes an increase in calcium influx and calpain2 phosphorylation, subsequently leading to MPST degradation. The PP2A activator (FTY720) and MPST activator (3MP sodium) both remarkably restored endothelial MPST-dependent H_2S production, subsequently rescuing ischemia-induced neurological deficits. In conclusion, our study demonstrates that endothelial PP2A deficiency leads to MPST degradation by activating calpain2, thus damaging neuronal function.

1. Introduction

Endothelial cells (ECs), pericytes, astrocytes, glia, and neurons comprise the neurovascular unit (NVU). The NVU relies on a delicate balance of communication between ECs and neurons to maintain structural integrity and proper functioning of the brain[1]. However, once endothelial dysfunction occurs, the intercellular communication is disrupted, potentially resulting in severe consequences.

Communication between ECs and neurons within the NVU depends on delicate signal transduction pathways, including the exosome, neurotransmitter, and gasotransmitter systems[2]. Gaseous messengers generated by the endothelium can exert their effects on neurons remotely from the site of secretion, owing to their rapid diffusion. Research has demonstrated that hydrogen sulfide (H_2S) derived from the endothelium safeguards against neuronal dysfunction by inhibiting the hyperphosphorylation of pathogenic proteins, reducing excitatory neural toxicity, and other underlying mechanisms[3]. The enzyme 3-mercaptopyruvate (3MP) sulfurtransferase (MPST) is widely expressed in the brain and facilitates the conversion of 3MP into H_2S[4]. Studies have demonstrated the neuroprotective effects of MPST through its antioxidant and anti-inflammatory properTies[5,6]. A previous study reported a decrease in MPST within the cerebrovascular system in paTients with acute ischemic stroke[7]. However, the role of MPST in brain disorders and the regulatory mechanisms governing its activity remain largely unknown.

Phosphorylation is a common post-translational modification that regulates protein function and activity. According to a tissue-specific atlas of mouse protein phosphorylation, the brain exhibited the highest abundance of phosphoproteins[8]. Additionally, a similar study unveiled that serine and threonine residues constituted the predominant phosphorylation sites among all phosphoprotein phosphorylation sites[9]. Protein phosphatase 2A (PP2A), a serine/threonine phosphatase, strictly controls the phosphorylation of tau and α-synuclein, thereby impeding the onset of Alzheimer's disease (AD) and Parkinson's disease. Notably, PP2A has been demonstrated to be inhibited in cognitive impairment disorders[10,11]. Both MPST and H_2S have been implicated in protein phosphorylation[12,13]. Hence, we postulated a potential synergistic interaction between MPST and PP2A to safeguard the functionality of the NVU.

Therefore, our study aimed to elucidate the role and mechanism of endothelial PP2A in modulating neuronal function and its association with MPST-derived H_2S. We found that endothelial PP2A maintained MPST-mediated H_2S production by inhibiting the activity of calpain2, which is necessary for preventing neuronal loss and cognitive dysfunction. The PP2A−MPST transduction pathway holds promise as a potential therapeutic target for mitigating cerebrovascular damage.

2. Materials and methods

2.1. Reagents and antibodies

Collagenase IV (40510ES60) was purchased from YEASEN (Shanghai, China), DNase I (D5025) was purchased from GBCBIO (Guangzhou, China), bFGF (450-33) was purchased from PeproTech (Cranbury, NJ, US), fibronectin (HY-P0306) was purchased from MedChemExpress (NJ, US), phosphatase assay kit (17-127) was purchased from Millipore (Darmstadt, Germany), Evans blue solution (314-13-6) and NaHS (161527) were purchased from Sigma−Aldrich (Darmstadt, Germany). Fura-2/AM (F1225) was purchased from Invitrogen (Darmstadt, Germany), NaHS (161527) was purchased from Sigma−Aldrich (Darmstadt, Germany), FTY720 (S5950) was purchased from Selleck (Houston, US).

The antibodies used in the study are listed below: anti-PP2Acα (106334) was purchased from GeneTex (SAN Antonio, TX, US), anti-CBS (sc-133154), anti-CSE (sc-374249), anti-MPST (sc-376168), anti-calpain 2 (sc-2539), anti-β-actin (sc-58673), anti-calpain 1 (sc-2556), and anti-P-ser (sc-81514) were purchased from Santa Cruz (TX, US), anti-Neun (24307), horseradish peroxidase (HRP)-conjugated anti-rabbit/mouse IgG (7074S/14709) were purchased from Cell Signaling Technology (Danvers, MA, US), donkey-anti-rabbit IgG Alexa Fluor 488 (A-21206), donkey-anti-rabbit IgG Alexa Fluor 555 (A-31572) and donkey-anti-mouse IgG Alexa Fluor 488 (A-21202) were purchased from Invitrogen (Darmstadt, Germany), Goat-anti-rabbit IgG Alexa Fluor 647 (Abcam, ab150079) and Goat-anti-mouse IgG Alexa Fluor 647 (Abcam, 150115) were purchased from Abcam (Cambridge, UK).

2.2. Animals

All mice used for this study were housed and bred in specific pathogen-free conditions in the animal facility of the Guangzhou University of Chinese Medicine. *Ppp2ca* floxed ($Ppp2C\alpha^{f/f}$) and TIE 2-Cre animals were a munificent gift from Peking Union Medical College Hospital (Beijing, China). Mice were divided into individual cages and housed in SPF conditions with food and water. All experimental mice were C57BL/6 background. $Ppp2C\alpha^{f/f}$ mice crossed with Tie2-Cre to generate PP2A endothelial specific deficiency mice (Tie2-Cre, $PP2AC\alpha^{f/f}$; $PP2A^{EC\text{-}CKO}$), PCR genotyping was performed following the protocol by Peking Union Medical College Hospital. All experiments were performed following Guangzhou University of Chinese Medicine guidelines for animal research. All the procedures on mice were approved by the Ethics Review Board at Guangzhou University of Chinese Medicine Guidelines (Guangzhou, China; Approval No. ZYD-2020-151).

2.3. Cell lines

Mouse brain endothelial cells (bEnd.3 cells, CRL-2299, ATCC) were maintained with culture medium containing 10% FBS (GIBCO,10270-106), 1% Antibiotic-Antimycotic (GIBCO,15140-122) in DMEM (GIBCO,11995-065) at 37 °C in a 5% CO_2-humidified incubator. The cell line was obtained directly from ATCC, with no additional cell authentication performed.

2.4. Gene function and protein−protein interaction (PPI) networks analysis

Using Cluster Profiler, GO analysis was applied to decipher the biological nuances within the gene expression data[14]. Parameters, such as ontology type and *P*-value adjustment, can be meticulously fine-tuned. The finale arrives as a visual spectacle: bar plots vividly encapsulate the enriched GO terms, transforming complex data into actionable biological insights. Terms with a Benjamini−Hochberg corrected *P*-value of less than 0.05 were defined as key regulated pathways. In addition, the integration of the STRING database (version 12.0; https://string-db.org) and Cytoscape software (version 3.10.0; https://cytoscape.org) provided a streamlined approach for crafting and interpreting PPI networks[15,16]. Here, criteria in the interaction score, set as medium confidence (0.40), and interaction sources, including text mining, experiments, databases, co-expression, neighborhood, gene fusion, and cooccurrence, were used to export the generated network. Transitioning to Cytoscape and selecting a visual layout that suits analytical requirements, nodes and edges can be customized for easier interpretation, and Cytoscape's analytics provide insights into key network components[17]. This unified process transforms intricate protein interactions into a comprehensible and actionable landscape, offering invaluable perspectives for research and practical applications. Of the hub regulators, the compartmentalized PPI database (version 2.1.1; ComPPI; http://comppi.linkgroup.hu)[18] and graph algorithm[19] were applied to construct the regulators' subcellular localizations of the interaction network. Employing IGraph's suite of analytical tools, we identified core molecules based on various network metrics, such as degree and betweenness. These core entiTies were then cross-referenced with their subcellular localizations from COMPPI, allowing us to pinpoint where these crucial interactions occur within the cell. Finally, we visualized the network using iGraph to accentuate the core molecules and their subcellular realms.

2.5. Primary mouse brain endothelial cells isolation

Mouse primary brain microvascular endothelial cells (PBMECs) were isolated and cultured from 3 to 4 weeks male mice using other previously described protocol[20] with little modification. In brief, the mice's cerebrum was isolated and removed free of the cerebellum, and brain stem and meninges. The cerebrum was dissected, and minced finely with scissors, pipette the tissue fragments up and down until no clumps appeared. Then digested tissue fragments for 2 h at 37 °C on a rotator with DMEM containing 4% 10 mg/mL collagenase IV, 5.3% 0.25 mg/mL DNase I, 0.9% 1 mol/L HEPES, 5 mmol/L Ca^{2+}, with gentle trituration every 10 min. Following adequate digestion and centrifugation at 1000 × *g* for 10 min, the cell pellets were resuspended in 20% BSA and then subjected to centrifugation at 1000 × *g* at 4 °C for 20 min. Then, cell pellets were resuspended in EC culture medium (DMEM with 20% FBS, 20 mg/mL basic fibroblast growth factor (bFGF), 100 mg/mL heparin, and 4 mg/mL puromycin to a specific selection of brain ECs and plated into fibronectin-precoated plates (10 mg/mL at 37 °C for 30 min). After 3 days, the cells were washed with phosphate-buffered saline (PBS, pH 7.4) twice and then switched to an ECs culture medium without puromycin. Cells were collected for further experiment until the cell population became confluent.

2.6. RNA sequence analysis

Total RNA from PBMECs isolated from $PP2AC\alpha^{f/f}$ or $PP2A^{EC\text{-}CKO}$ mice was extracted using Trizol (Invitrogen, USA) following manufacturer's instruction. mRNA was purified from total RNA using poly-T oligo-attached magnetic beads. The clustering of the index-coded samples was performed on a cBot Cluster Generation System using TruSeq PE Cluster Kit v3-cBot-HS (Illumia) according to the manufacturer's instructions. After cluster generation, the library preparations were sequenced on an Illumina Novaseq platform (Novogene, Beijing, China) and 150 bp paired-end reads were generated. Reads were mapped to the Mus musculus genome with the Hisat2 v2.0.5 identified the differentially expressed genes (DEG). Differential expression analysis of two groups (three biological replicates per group) was performed using the DESeq2 R package (1.20.0). Genes with an adjusted *P*-value <0.05 found by DESeq2 were assigned as differentially expressed. KEGG enrichment analysis of differentially expressed genes was implemented by the clusterProfiler R package, in which gene length bias was corrected.

2.7. Animal models

Bilateral carotid artery occlusion (BCAO) was performed as previously described[21]. Mice were anesthetized with isoflurane and secured on the surgical table. The animals' body temperature was maintained at 37.0 ± 0.5 °C using a heating blanket. Fur around the ventral neck region was removed with a hair clipper to expose the skin, which was then disinfected with iodine. Under the operating microscope, a midline incision in the ventral neck region was performed using a scalpel. The superficial fascia was dissected to expose the bilateral common carotid arteries. Subsequently, micro-vessel clamps were used to occlude the carotid arteries for 20 min to induce global cerebral ischemia, followed by

clamp removal and reperfusion for 1 week. The neck incision was closed with 5-0 sterile silk sutures. The mice were transferred to a warm (37.0 ± 1 °C) recovery chamber until fully awake.

Partial ligation on the left carotid artery (LCA) was performed as previously described[22]. Briefly, mice were anesthetized with isoflurane and securely positioned on the surgical table. The LCA was carefully exposed through blunt dissection. The left external carotid, internal carotid, and occipital artery were meticulously ligated using 6-0 silk suture. Subsequently, the incision was meticulously sutured. Throughout the procedure, the body temperature of the mice was maintained at 37.0 ± 0.5 °C until they fully recovered.

2.8. Drug administration

NaHS was prepared as a 15 mmol/L working solution in normal saline and stored at 4 °C. Normal saline was served as the vehicle control for control group mice. Male mice aged 8−10 weeks were randomly assigned to four groups: PP2AC$\alpha^{f/f}$ saline group, PP2AC$\alpha^{f/f}$ NaHS group, PP2A$^{EC\text{-}CKO}$ saline group, PP2A$^{EC\text{-}CKO}$ NaHS group. The mice were treated with NaHS (30 μmol/kg/day) or saline for 14 days *via* intraperitoneal injections, following previously described protocols[23] or saline for 14 days through intraperitoneal injections before performed behavioral tests.

FTY720 was dissolved in dimethyl sulfoxide and diluted in saline. Mice in the Sham or LCA group received FTY720 (2 mg/kg/day) or saline for 14 days by gavage according to previously described[24]. Mice in the Sham or LCA group were treated with 3MP sodium (1 mg/kg/day) or saline for 14 days *via* intraperitoneal injection according to a previous study[25].

2.9. Nissl staining

The cerebral tissues were dehydrated with gradient ethanol elution and cleared in xylene, coronal brain slices were sliced into 7 μm using a cryostat and stored at −20 °C. Nissl staining (Beyotime) was conducted according to the manufacturer's instructions. Briefly, the sections were incubated with 1% toluidine blue for 25 min at 37 °C, washed with double distilled water, and dehydrated with gradient ethanol elution. The slice sections were observed using the Olympus CX31 microscope (OLYMPUS), the number of staining cells was counted at 400 × magnification in a blinded manner, only structures of appropriate size and shape were demonstrated clearly.

2.10. Immunohistochemistry

Briefly, mice were euthanized, and then *trans*-cardiac perfused with saline, 4% PFA. Tissues were dissected out, fixed 24 h in 4% PFA, and then dehydrated in 15% and 30% sucrose in PBS. Coronal brain slices (30 μm) were prepared by using a vibratome (thermo). The sections were incubated with 0.3% Triton X-100 in PBS for 20 min and blocked for 1 h in 10% donkey serum in PBS at RT. For immunolabeling, the brain sections were then incubated with primary antibodies overnight at 4 °C and then incubated in Alexa Fluor-conjugated secondary antibodies (Invitrogen) for 2 h at 37 °C. Sections were mounted and images were obtained by using the Nikon A1 laser-scanning confocal microscope (Nikon).

2.11. PP2A activity assay

PP2A activity was evaluated as previously described[26]. Cell lysates from PBMECs or bEnd.3 Cells infected with lenti-Ppp2ca-shRNA or lenti-vector were subjected to PP2A immunoprecipitation (IP) using anti-PP2A catalytic subunit (PP2AC) antibody (cell signaling technology, 2238S) overnight at 4 °C, followed by immobilization on protein A/G magnetic beads (MCE HYK, 0202) for 2 h. The immunoprecipitate was then incubated with phosphopeptide substrate (KRpTIRR) for 30 min at 37 °C, and the reaction was terminated using Malachite green reagent before measuring the absorbance at 620 nm.

2.12. Measurement of blood−brain barrier (BBB) permeability

The measurement of BBB permeability was according to previously described[27] with little modification. Mice were intravenously injected with 80 mg/kg of Evans blue solution (Sigma−Aldrich, St. Louis, MO, USA) *via* the tail vein. Two hours later, the mice were euthanized and perfused with ice-cold PBS. The brains were then extracted and placed in 1 mL of formamide. Subsequently, the samples were incubated at 60 °C for 48 h, and absorbance readings of the supernatant were taken at OD 620 nm. A standard curve was generated using known concentrations of Evans blue dye in formamide to calculate the concentration of Evans blue.

2.13. Measurement of cerebral blood flow

Cerebral blood flow in the mouse cortex was assessed using laser Doppler imaging (PeriScan PIM 3 System, PERIMED). CBF measurements were obtained before and during bilateral common carotid artery occlusion (BCAO), as well as 2 min after reperfusion.

2.14. AAV viral injection

An AAV vector carrying a Tie promoter was employed to induce the expression of Cre, *Ppp2ca*, and *Mpst* in the endothelium. The recombinant plasmids AAV9-Tie-Cre (1.7×10^{12} vg/mL), AAV9-Tie-*Ppp2ca* (1.7×10^{12} vg/mL), and AAV9-Tie-MPST (1.8×10^{12} vg/mL) were constructed, amplified, and purified by Hanbio Biotechnology (Shanghai, China). AAV9-Tie-Cre was injected into PP2AC$\alpha^{f/f}$ mice for brain endothelial *Ppp2ca* deletion. AAV9-Tie-*Ppp2ca* and AAV9-Tie-*Mpst* were administered into PP2AC$\alpha^{f/f}$ and PP2A$^{EC\text{-}CKO}$ mice for overexpression of *Ppp2ca* or *Mpst*, respectively. For viral delivery, one-month-old PP2AC$\alpha^{f/f}$ and PP2A$^{EC\text{-}CKO}$ mice were anesthetized with 2% isoflurane and positioned on a stereotaxic setup. Bilateral injection of a total of 0.4 μL virus into the hippocampus (4×10^{11} vg/hippocampus) at a rate of 0.1 μL/min three weeks before behavioral tests. Two injection sites per hippocampus were used to optimize viral spread. Stereotactic coordinates of injection sites from bregma were: DG (AP, −1.9 mm from bregma; ML, ±1 mm; DV, −2.25 mm) and CA3 (AP, −1.7 mm from bregma; ML, ±2.0 mm; DV, −2.12 mm).

Recombinant plasmids AAV-BR1-Tie-Cre (1×10^{13} vg/mL), AAV-BR1-Tie-Ppp2ca (1×10^{13} vg/mL), AAV-BR1-Tie-*Mpst* (1×10^{13} vg/mL), AAV-PHP.eb-*Hsyn*-Cre-EGFP (1×10^{13} vg/mL), and AAV-PHP.eb-*Gfap*-Cre- EGFP (1×10^{13} vg/mL) were constructed, amplified, and purified using PackGene Biotech (Wuhan, China). The virus was diluted to a concentration of 3×10^{11} vg/mL with PBS and intravenously injected into PP2AC$\alpha^{f/f}$ and PP2A$^{EC\text{-}CKO}$ mice.

2.15. Behavioral tests

The Y-maze consisted of three Plexiglas arms of equal size joined together in a Y configuration. Each arm measured 40 cm in length, 10 cm in width, and had 12-cm-high walls. The floor of each arm was made of blue plastic, while the walls were constructed from clear plastic. The apparatus was positioned on the floor of the experimental room and illuminated with a 100-Watt bulb from a height of 200 cm. Each trial comprised two exposures to the maze. Initially, mice were permitted to explore two out of the three arms for a total duration of 5 min, while the third arm (novel arm) remained blocked off. Subsequently, after 30 min had elapsed, mice were returned to the same starting point within the maze and allowed to freely explore for 3 min with all arms open. The percentage of time spent in the novel arm was then recorded.

The Morris Water Maze was utilized to assess hippocampus-dependent spatial reference memory. In the hidden platform trial, the platform was positioned at the center of one of the four quadrants of the pool (DigBehv), submerged 1 cm below the water surface. Mice underwent four 90-s acquisition trials to locate the hidden platform with a 30 min inter-interval per day for five consecutive days. Mice that successfully found the platform were allowed to remain on it for 10 s. The average time taken to find the platform and the swimming path were both recorded. On Day 6, a probe test was carried out, during which mice were placed into water in the opposite quadrant of their goal and allowed to swim freely for 90 s without access to the platform. The average time spent in their goal quadrant was recorded.

Novel object recognition (NOR) test was performed according to a previous study[28]. Briefly, open field arena (40 cm × 40 cm × 40 cm) was applied in the test. The NOR test consisted of an acquisition phase and a testing phase. During the acquisition phase, two identical objects (height: 10 cm; base diameter: 6 cm) were affixed to the open field arena. Mice were placed at the center of the arena and allowed to freely explore for 5 min. A testing phase lasting 5 min was conducted 2 h after the acquisition phase. In this phase, one of the objects was replaced with a novel object measuring 4 cm × 4 cm × 8 cm. Mice were again placed at the center of the arena and allowed to freely explore for another 5 min. The time spent exploring both familiar and novel objects was recorded and analyzed. The apparatus was cleaned with 20% ethanol after each test, and a discrimination index [(novel object time)/(novel object time + familiar object time)] was calculated for analysis purposes.

2.16. Field EPSP recordings of hippocampal slices

The mice were deeply anesthetized and then underwent transcardial perfusion with ice-cold sucrose-rich slicing solution. The slicing solution consisted of the following concentrations (in mmol/L): 85 NaCl, 2.5 KCl, 4 $MgCl_2$, 0.5 $CaCl_2$, 1.25 NaH_2PO_4, 25 $NaHCO_3$, 25 glucose, and 75 sucrose. Prior to perfusion, the slicing solution was oxygenated with a mixture of 95% O_2 and 5% CO_2. The brain was promptly extracted and placed in a sucrose-rich slicing solution. Slices (256 μm) were then precision-cut using a Leica VT1200s vibratome, followed by a 1 h recovery period at 35 °C in oxygenated artificial cerebrospinal fluid (ACSF; containing 119 mmol/L NaCl, 2.5 mmol/L KCl, 1.3 mmol/L $MgCl_2$, 2.5 mmol/L $CaCl_2$, 1.25 mmol/L NaH_2PO_4, 1.3 mmol/L $NaHCO_3$, and 10 mmol/L glucose). Subsequently, the slices were maintained at 25 °C for an additional hour before electrophysiological recordings took place.

Slices were transferred to the recording chamber and perfused with oxygenated ACSF at a rate of approximately 3 mL/min. The slices were visualized using infrared optics with an upright microscope equipped with a 60 × water-immersion lens (ECLIPSE FN1, Nikon). Pyramidal neurons were identified based on their cell body morphology and location. A glass microelectrode filled with ACSF was positioned in the CA1 stratum radiatum to record field excitatory postsynaptic potentials (fEPSPs). fEPSPs were evoked with an intensity of 0.2 ms, which elicited approximately 50% of the maximum amplitude at a frequency of 0.05 Hz. Long-term potentiation (LTP) was induced using a high-frequency stimulation (HFS) protocol consisting of two consecutive trains of stimuli at 100-Hz pulses with 20 s intervals. Potentiation was calculated as the percentage increase in average fEPSP slopes during the last 10 min normalized to the average baseline slopes. Signals were acquired using a MultiClamp 700B amplifier, filtered at 2 kHz, and sampled at 10 kHz with a Digidata 1440A interface. Data were obtained with Clampex 10.2 software and analyzed with Clampfit 10.2.

2.17. Lentivirus transduction

The *lenti-Ppp2ca-shRNA* plasmid was constructed and purchased from Fubio Biology Technology (Shuzhou, China). To achieve *Ppp2ca* knockdown in bEnd.3 cells, lentivirus transduction of shRNA targeting the *Ppp2ca* sequence (5′-GACTATCATATGCTTACCGT-3′) was performed. Briefly, cells were incubated with lentiviral particles at a multiplicity of infection (MOI) of 100 in DMEM medium supplemented with 10% heat-inactivated FBS, 1% P/S, and 1 × LV-Enhance surfactant. After 24 h, the cells were washed and then incubated in regular growth medium. Following a resting period of 24 h, successfully infected cells were screened using 3 μg/mL puromycin. Subsequent analysis was conducted 32 h after puromycin treatment.

2.18. Co-immunoprecipitation

Immunoprecipitation of calpain2 and MPST conducted using lysate prepared from control and $PP2A^{EC\text{-}CKO}$ PBMECs, cells were lysed in 300 μL RIPA buffer (50 mmol/L Tris, pH 8.0, 150 mmol/L NaCl, 0.1% SDS, 1.0% NP-40, 0.5% sodium deoxycholate, and protease inhibitor cocktail; Roche), sheared with a sonication device, and centrifuged at 12,000 × *g* at 4 °C for 20 min. The supernatants were then incubated with the appropriate antibody (1:100), anti-calpain2, anti-calpain1 or anti-MPST overnight at 4 °C, followed by incubation with 50 μL magnetic beads for 2 h at 4 °C. Subsequently, the beads were washed five times with 1 × RIPA buffer. 32 μL 1 × RIPA and 8 μL protein loading buffer were added to the beads, followed by heating at 95 °C for 5 min. Samples were processed for immunoblotting to analyze the interactions between immunoprecipitated proteins.

2.19. Western blotting

All samples were lysed in RIPA buffer. Samples containing equivalent amounts of protein were then subjected to SDS-Page gel electrophoresis and transferred to a nitrocellulose membrane. Membranes were blocked with 5% milk, incubated with the following primary antibodies at 4 °C overnight, and then incubated with HRP conjugated secondary antibodies. The proteins were visualized by an enhanced chemiluminescence detection

system (Millipore). Quantification of the bands was performed using ImageJ software (National Institutes of Health, USA), and results were normalized against the corresponding β-actin band used as loading control.

2.20. Real-time PCR analysis

Total RNA was extracted by trizol (Takara, 9109). cDNA was generated from 2 μg RNA using PrimeScript RT Regent kit (Takara), and real-time PCR analyses were performed with SYBR Green Master Mix using the Thermo 7300 Real-Time PCR Detection System (Thermo Scientific). The mRNA level of target genes was normalized to that of the housekeeping gene GAPDH. Genes specific primers were designed by Primer Bank and listed as follows:

Mouse *Gapdh*: Forward: 5′-AGGTCGGTGTGAACGGATTTG-3′,

Reverse: 5′- GGGGTCGTTGATGGCAACA-3′;

Mouse *Mpst*: Forward: 5′- TCACAGCCGCTGAAGTTACTG-3′,

Reverse: 5′- CAGCATGTGGTCGTAGGGG-3′;

Mouse *Capn2*: Forward: 5′- GGTCGCATGAGAGAGCCATC-3′,

Reverse: 5′- CCCCGAGTTTTGCTGGAGTA-3′;

Mouse *Capn1*: Forward: 5′- ATGACAGAGGAGTTAATC ACCCC -3′,

Reverse: 5′- GGCTATGAGAAACCGGAGGG -3′.

2.21. Measurement of H_2S concentration

H_2S concentration was analyzed using commercial kits from Nanjing Jiancheng Biology (Nanjing, China) following the manufacturer's protocol.

2.22. Calcium image

Calcium influx were monitored by using 1 μmol/L Fura-2/AM (Invitrogen, F1225) as previously described[29] with minor modification. PBMECs from control or $PP2A^{EC\text{-}CKO}$ mice were incubated for 40 min in the dark at 37 °C, then rinsed with saline and incubated with Hank's buffered saline solution (pH 7.4) for an additional 20 min. The cells were imaged on a Zeiss microscope equipped with a cell stretching device. Fura-2 was excited using a 340 and 380 nm filter wheel, and images were captured every 10 s with a camera using Flexstation3 (Molecular Devices). Baseline recordings were taken for 3 min before the addition of 100 μL of 0.3 mol/L $CaCl_2$. Cells were considered responsive if the peak Fura-2 ratio after stretch was at least 50% higher than the mean baseline value, and imaging continued for an additional 30 min. Data acquisition was performed using Metaflour software (Molecular Devices).

2.23. Statistical analysis

Mice were randomized for experimental conditions using Microsoft Excel. Data analysis was performed with GraphPad Prism 8.0 in a blinded fashion, and normal distribution was tested with the *Shapiro−Wilk* test. Group comparisons were made using log-rank, one-way ANOVA, two-way ANOVA, and Mann−Whitney *U* test. Data are presented as mean ± standard error of mean (SEM), and differences are considered statistically significant at $P < 0.05$.

3. Results

3.1. Endothelial PP2A deficiency induces hippocampal neuron dysfunction in mice

The neuroprotective role of PP2A has been extensively documented; however, further investigation is required to elucidate its impact on crosstalk between ECs and neurons. Our study sought to identify the molecular pathway that interacts with PP2A and influences communication between ECs and neurons. Genes related to vascular cognitive impairment disease were retrieved from DisGeNET and GeneCards datasets. The regulatory roles of H_2S and protein phosphatase, particularly PP2A, were highlighted through GO enrichment analysis and PPI network analysis using ClusterProfiler and STRING (Fig. 1A−C). To further confirm the role of PP2A in orchestrating EC-neuron crosstalk in a pathological state, we generated PP2A EC-specific deficiency mice (Tie2-Cre; $PP2AC\alpha^{f/f}$, hereafter referred to as $PP2A^{EC\text{-}cKO}$) by crossing $Ppp2C\alpha^{f/f}$ mice with Tie2-Cre mice, followed by identification to confirm the deletion of *Ppp2Cα* (Supporting Information Fig. S1A−S1E) and inactivation of PP2A (Supporting Information Fig. S1F and S1G) in brain endothelium. Primary brain microvascular ECs (PBMECs) isolated from $PP2AC\alpha^{f/f}$ and $PP2A^{EC\text{-}cKO}$ mice were harvested for RNA sequencing analysis. Enrichment analysis revealed that endothelial PP2A deficiency was involved with pathways of neurodegeneration in multiple diseases (Fig. 1D). Furthermore, the partial ligation on the left carotid artery (LCA) model was performed to induce cerebral ischemia. A significant decrease in PP2Acα expression was detected in PBMECs isolated from mice subjected to LCAcompared with that in sham (Fig. 1E). Further, a robust reduction of PP2ACα protein expression was observed in the vascular endothelium in LCA mice (Fig. 1F and G). The survival of $PP2A^{EC\text{-}cKO}$ mice was notably reduced by LCA, while $Ppp2C\alpha^{f/f}$ mice remained unaffected (Fig. 1H). Compared with observations of control mice, both $PP2A^{EC\text{-}cKO}$ and ligated $PP2A^{EC\text{-}cKO}$ mice showed decreased preference for the novel arm (poor spatial cognition) during the Y-maze test (Fig. 1I), increased latency to find the hidden platform (impaired learning ability), and reduced duration in the goal quadrant in probe trials (impaired memory ability) in the Morris water maze test (Fig. 1J−L). Furthermore, a reduction of Nissl bodies and $NeuN^+$ neurons was found in the hippocampus and cortex of $PP2A^{EC\text{-}cKO}$ mice (Fig. 1M−O; Supporting Information Fig. S2K and S2L). Compared to the increase in extracellular field excitatory postsynaptic potentials and long-term potentiation (LTP) response induced by high-frequency stimulation in hippocampal slices derived from $PP2AC\alpha^{f/f}$ mice, the $PP2A^{EC\text{-}cKO}$ slices exhibited a diminished propensity for maintaining LTP (Fig. 1P). The averaged field excitatory postsynaptic potential slope during the last 10-min period of LTP was significantly lower in $PP2A^{EC\text{-}cKO}$ compared with that in $PP2AC\alpha^{f/f}$ slices (Fig. 1Q). In addition, female $PP2A^{EC\text{-}cKO}$ mice exhibited similar neurological defects (Fig. S2A−S2D), thereby excluding the effects of sex differences. To confirm the protective role of endothelial PP2A in cerebral ischemia, bilateral common carotid artery occlusion (BCAO) was performed to induce hypoperfusion. Endothelial PP2A deficiency increased the mortality rate in mice undergoing BCAO surgery (Fig. S2E). Furthermore, BCAO exacerbated neuronal dysfunction in $PP2A^{EC\text{-}cKO}$ mice (Fig. S2F−S2J). Collectively, these data suggest that endothelial PP2A deficiency induces neuronal loss and cognitive dysfunction.

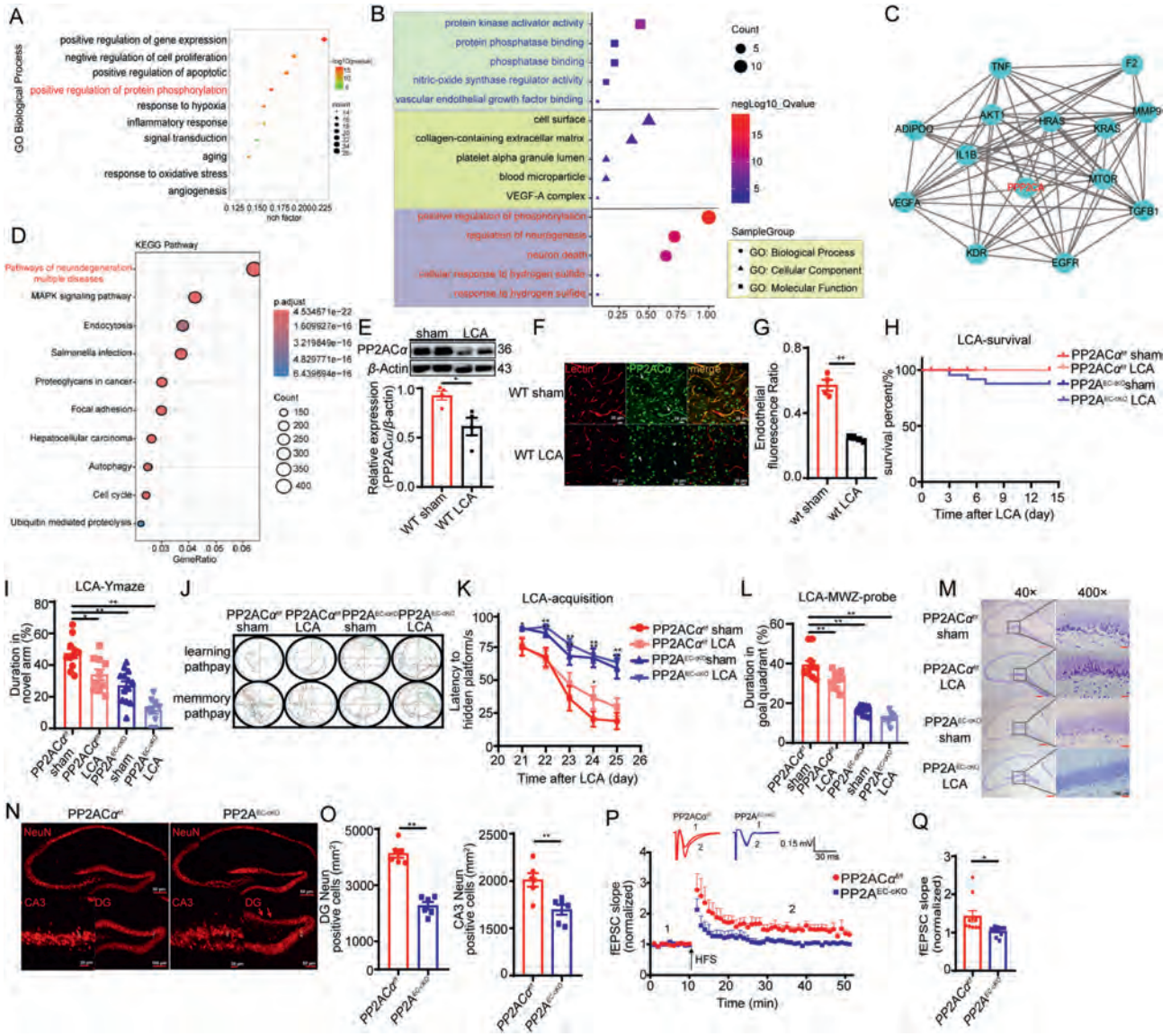

Figure 1 Endothelial PP2A deficiency induces hippocampal dysfunction in mice. (A−C) Bioinformation analysis. Gene Ontology (GO) biological process analysis of genes related to VCD (A, B). Protein interaction network of genes enriched in "positive regulation of protein phosphorylation", "response to hydrogen sulfide" and PP2ACA *via* STRING (C). (D) Kyoto Encyclopedia of Genes and Genomes (KEGG) pathway analysis of different genes in RNA sequencing ($n = 3$). (E) Immunoblots of PP2ACα proteins level in PBMECs isolated from WT sham or WT LCA mice ($n = 4$). (F, G) Representative confocal image (F) and quantification (G) of PP2ACα in brain endothelium of wild type mice after LCA, PP2Acα (Green), lectin + endothelium (red) ($n = 4$). Scale bar, 20 μm. (H) Survival curves of PP2A$^{EC\text{-}cKO}$ *versus* PP2AC$\alpha^{f/f}$ mice after partial ligation on left carotid artery (LCA). (I−L) Cognition of male mice was evaluated by Y-maze test (I) and Morris water maze test 28 days after LCA. (J) The typical swim path of mice in the Morris water maze test. (K) Latency to reach the hidden platform during the acquisition trial after LCA. (L) Percentage occupancy in the goal quadrant in the probe trial ($n = 10$−13). (M) Nissl staining for neurodegeneration in the hippocampus after LCA ($n = 5$). (N, O) Representative confocal image (N) and quantification (O) of NeuN^{+} neurons (red) in the CA3 and DG hippocampal subfield of PP2AC$\alpha^{f/f}$ and PP2A$^{EC\text{-}cKO}$ mice ($n = 6$). Scale bar, 20 or 50 μm. (P, Q) Reduced hippocampal fEPSP slope (P) and averages of the last 10 min of fEPSP recording(Q) in the CA1 region of PP2A$^{EC\text{-}cKO}$ mice compared to PP2AC$\alpha^{f/f}$ mice. Representative traces before (1) and after (2) tetanic stimulation was shown above fEPSP recording. Scale bars depict 10 ms or 0.25 mV. PP2AC$\alpha^{f/f}$: $n = 10$ from 4 mice; PP2A$^{EC\text{-}cKO}$: $n = 10$ from 3 mice. Data are expressed mean ± SEM, $^{*}P < 0.05$, $^{**}P < 0.01$.

3.2. PP2A deficiency in brain endothelium via AAV-Tie-Cre also induces cognitive dysfunction

To exclude the possibility that neuronal dysfunction in PP2A$^{EC\text{-}cKO}$ mice was caused by peripheral endothelial PP2A deficiency, we generated EC-targeted AAV (AAV9-Tie-Cre) *via* bilateral stereotaxic injections into the brains of PP2AC$\alpha^{f/f}$ mice to delete *Ppp2cα* solely in brain ECs. Fig. 2A illustrates the AAV injection process. AAV9-Tie-Cre induced a robust reduction of PP2ACα expression in the hippocampal vasculature (Fig. 2B and C). Significant defects in the cognitive function of PP2AC$\alpha^{f/f}$ mice injected with AAV9-*Tie*-Cre were observed both in the Y-maze

and Morris water maze compared with the performance of control mice (Fig. 2D−G). Moreover, the AAV9-Tie-Cre injection decreased the number of Nissl bodies (Fig. 2H) and NeuN^{+}-positive cells (Fig. 2I and J) in the hippocampus. AAV-BR1-Tie-Cre and AAV-PHP.eb-*Hsyn*-Cre-EGFP, as well as AAV-PHP.eb-*Gfap*-Cre-EGFP, were intravenously injected into PP2AC$\alpha^{f/f}$ mice to delete *Ppp2cα* solely in brain microvasculature ECs, neurons and astrocytes, respectively. Cognitive function and neuronal loss were compared among the three knockout mice three weeks after virus injection. Significant cognitive dysfunction in the three PP2Ac*α* knockout mice was observed both in the novel object recognition (NOR) test and Y-maze compared with the performance of control mice (Supporting Information Fig. S3A−S3C). The cortex, CA3, and DG also showed a reduced number of NeuN^{+}-positive cells (Fig. S3D−S3E). Notably, the PP2AC$\alpha^{f/f}$ mice injected with AAV-BR1-Tie-Cre exhibited more defects in NOR, Y-maze performance, as well as cortical and CA3 neuron loss compared with those in the other two PP2A cKO mice. Collectively, these results support the notion that brain endothelial PP2A is necessary for the regulation of memory and neuronal viability.

3.3. Restoration of endothelial PP2A in the brain impedes cognitive dysfunction in PP2A$^{EC\text{-}cKO}$ mice

To further confirm the neuroprotective effects of endothelial PP2A, AAV9-Tie-*Ppp2ca* and AAV-BR1-*Tie*1.EGFP.2A-m*Ppp2ca* (BR1-Ppp2ca) were used to overexpress brain vascular endothelial *Ppp2cα via* bilateral stereotaxic and intravenous injection. Three weeks after AAV injection, we observed a significant increase in Ppp2ca expression in the endothelium (Fig. 3A and B; Supporting Information Fig. S4A and S4B). Furthermore, comparison to the performance of PP2A$^{EC\text{-}cKO}$ mice, the overexpression of *Ppp2cα* effectively reversed the cognitive dysfunction observed in NOR tests (Fig. S4C and S4D), Y-maze (Fig. 3C and Fig. S4E), and Morris water maze trials (Fig. 3D−F). Moreover, the number of Nissl

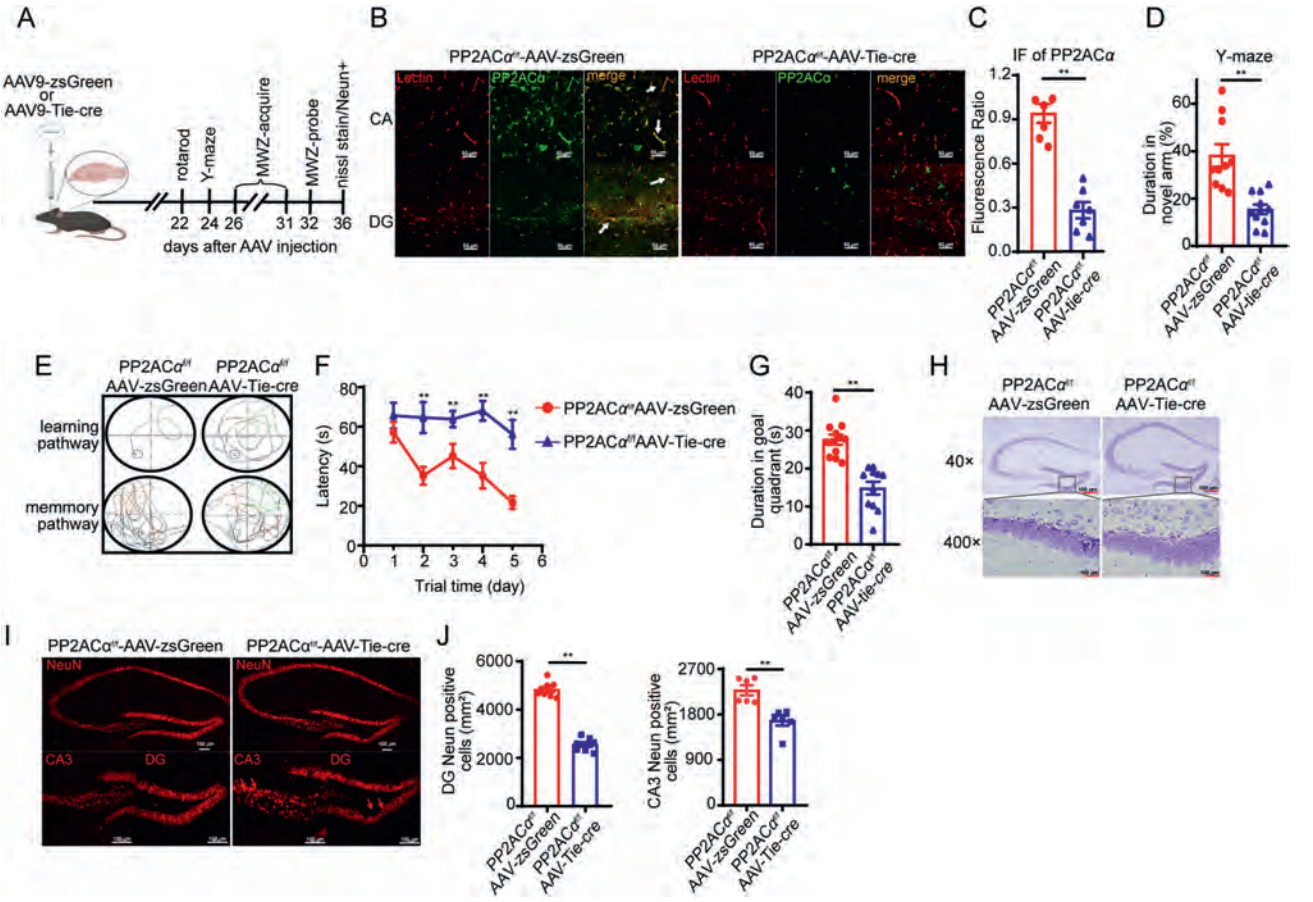

Figure 2 PP2A deficiency in brain endothelium *via* AAV-Tie-Cre also induces cognitive dysfunction. (A) Experimental schematic of AAV-Tie-Cre intrahippocampal injection. (B, C) Representative confocal image (B) and transduction ratio (C) of *Ppp2Cα* deletion in hippocampal endothelium at 3 weeks after AAV-Tie-CRE injection. PP2Ac$\alpha^{f/f}$ mice injected with AAV-Tie-CRE or AAV-zsGreen as control. PP2ACα(Green), lectin + endothelium (red) (n = 6−7). Scale bar, 50 μm. (D−G) Cognition was evaluated by Y-maze test (D) and Morris water maze test (E−G) at 3 weeks after AAV-Tie-CRE injection. (E) The typical swim path of PP2Ac$\alpha^{f/f}$-zsGreen and PP2Ac$\alpha^{f/f}$-AAV-Tie-cre mice in the Morris water maze test. (F) Latency to reach the hidden platform during the acquisition trial. (G) Percentage occupancy in the goal quadrant in the probe trial, (n = 10−11). (H) Nissl staining for neurodegeneration in the hippocampus of PP2Ac$\alpha^{f/f}$-zsGreen and PP2Ac$\alpha^{f/f}$-AAV-Tie-cre mice at 3 weeks after AAV-Tie-CRE injection, (n = 5). (I, J) Representative confocal image (I) and quantification (J) of NeuN^{+} neurons (red) in the CA3 and DG hippocampal subfield of PP2Ac$\alpha^{f/f}$-zsGreen and PP2Ac$\alpha^{f/f}$-AAV-Tie-cre mice at 3 weeks after AAV-Tie-CRE injection (n = 6−8). Scale bar, 50 μm. Data are expressed mean ± SEM, *P < 0.05, **P < 0.01.

bodies (Fig. 3G) and NeuN^{+} positive cells (Fig. 3H and I, Fig. S4F and S4G) in PP2A$^{EC\text{-}cKO}$ mice exhibited a significant increase following the restoration of PP2A activity in brain ECs. Together, these results further confirm that brain endothelial PP2A is crucial for impeding neuronal loss and cognitive dysfunction.

3.4. Endothelial PP2A deficiency resulted in a reduction of H_2S production in mice

To explore the neuroprotective mechanism of endothelial PP2A, its effect on the blood−brain barrier (BBB) and cerebral blood flow (CBF) were studied. However, endothelial PP2A deficiency did not alter BBB permeability to the small exogenous tracer Evans blue (Supporting Information Fig. S5A and S5B). This may be due to the dual effects of PP2A on the tight junctions. PP2A inactivation dramatically increased ZO-1 expression but reduced VE-cadherin (Fig. S5C). In addition, CBF also did not differ between the PP2A$^{EC\text{-}cKO}$ and PP2AC$\alpha^{f/f}$ mice (Fig. S5D and S5E). Bioinformatics analysis was used to identify molecules in the membrane, cytoplasm, and nucleus that may interact with PP2A (Fig. 4A). GO enrichment analysis results showed that PP2A influenced several H_2S-related signaling pathways, including 'disulfide oxidoreductase activity,' 'oxidoreductase activity,' 'protein disulfide isomerase activity,' and so on (Fig. 4B). Therefore, we decided to delineate the interaction between endothelial PP2A and H_2S. Notably, H_2S levels were significantly reduced in PP2A-deficient PBMECs (Fig. 4C and D). Meanwhile, knockdown of *Ppp2ca* also reduced the H_2S concentration in bEnd.3 cells (Fig. 4E). Consistently, exogenous H_2S (NaHS, a donor of H_2S) treatment dramatically improved cognitive function in

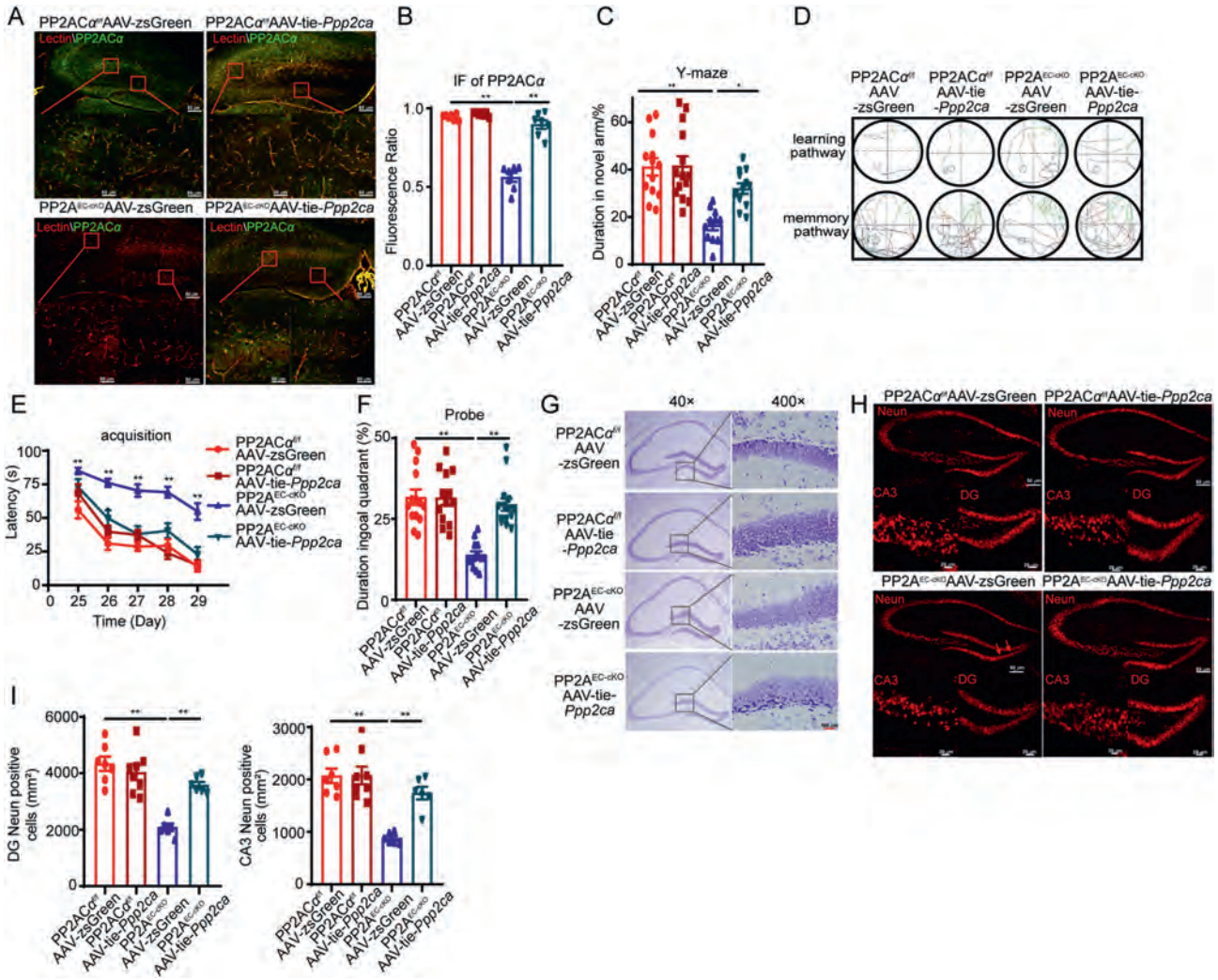

Figure 3 Restoration of endothelial PP2A in the brain impedes cognitive dysfunction in PP2A$^{EC\text{-}cKO}$ mice. (A, B) Representative confocal image (A) and ratio of *Ppp2Cα* restoration in hippocampal endothelium (B) at 3 weeks after AAV virus injection. PP2Acα (Green), lectin^{+} (red) is the marker of endothelium (n = 6−7). Scale bar, 50 μm. (C)−(F) Cognition was evaluated by Y-maze test (C) and Morris water maze test (D)−(F) at 3 weeks after AAV virus injection. (D) The typical swim path of PP2ACα$^{f/f}$-zsGreen, PP2ACα$^{f/f}$-AAV-Tie-*Ppp2cα*, PP2A$^{EC\text{-}cKO}$-zsGreen, PP2A$^{EC\text{-}cKO}$-AAV-Tie-*Ppp2cα* mice in the Morris water maze test. (E) Latency to reach the hidden platform during the acquisition trial. (F) Percentage occupancy in the goal quadrant in the probe trial (n = 11−14). (G) Nissl staining for neurodegeneration in the hippocampus of PP2ACα$^{f/f}$-zsGreen, PP2ACα$^{f/f}$-AAV-Tie-*Ppp2cα*, PP2A$^{EC\text{-}cKO}$-zsGreen, PP2A$^{EC\text{-}cKO}$-AAV-Tie-*Ppp2cα* mice at 3 weeks after AAV virus injection (n = 5). Scale bar, 100 μm. (H, I) Representative confocal image (H) and quantification (I) of NeuN^{+} neurons (red) in the CA3 and DG hippocampal subfield of PP2ACα$^{f/f}$-zsGreen, PP2ACα$^{f/f}$-AAV-Tie-*Ppp2cα*, PP2A$^{EC\text{-}cKO}$-zsGreen, PP2A$^{EC\text{-}cKO}$-AAV-Tie-*Ppp2cα* mice at 3 weeks after AAV virus injection (n = 6−8). Scale bar, 20 or 50 μm. Data are expressed mean ± SEM, $^{*}P < 0.05$, $^{**}P < 0.01$.

PP2A$^{EC\text{-}cKO}$ mice (Fig. 4F−I). Moreover, exogenous H_2S restored the number of Nissl bodies (Fig. 4J) and NeuN$^+$-positive cells in the hippocampi of PP2A$^{EC\text{-}cKO}$ mice (Fig. 4K and L). These results indicate that impaired endothelial H_2S production is implicated in the neuronal dysfunction associated with PP2A deficiency.

3.5. Reduction of H_2S is associated with suppression of endothelial MPST expression in PP2A$^{EC\text{-}cKO}$ mice

This study investigated the potential impact of PP2A deficiency on the expression of enzymes involved in H_2S biosynthesis. Notably, a robust reduction of MPST expression was found in the hippocampal vasculature of PP2A$^{EC\text{-}cKO}$ mice (Fig. 5A−D and Supporting Information Fig. S6A−S6C), PP2A deficient PBMECs, and Ppp2ca knockdown bEnd.3 cells (Fig. 5E and G). Additionally, inhibition of PP2A activity in bEnd.3 cells *via* its inhibitor, okadaic acid (100 nmol/L), led to a reduction in MPST protein levels (Fig. 5F). Restoration of PP2A activity in ECs using EC-targeted AAV-Ppp2ca significantly restored MPST expression (Fig. S6D−S6H) and H_2S production (Fig. S6I). However, endothelial PP2A deficiency showed little effect on the expression of the other two H_2S biosynthesis enzyme, CSE (Supporting

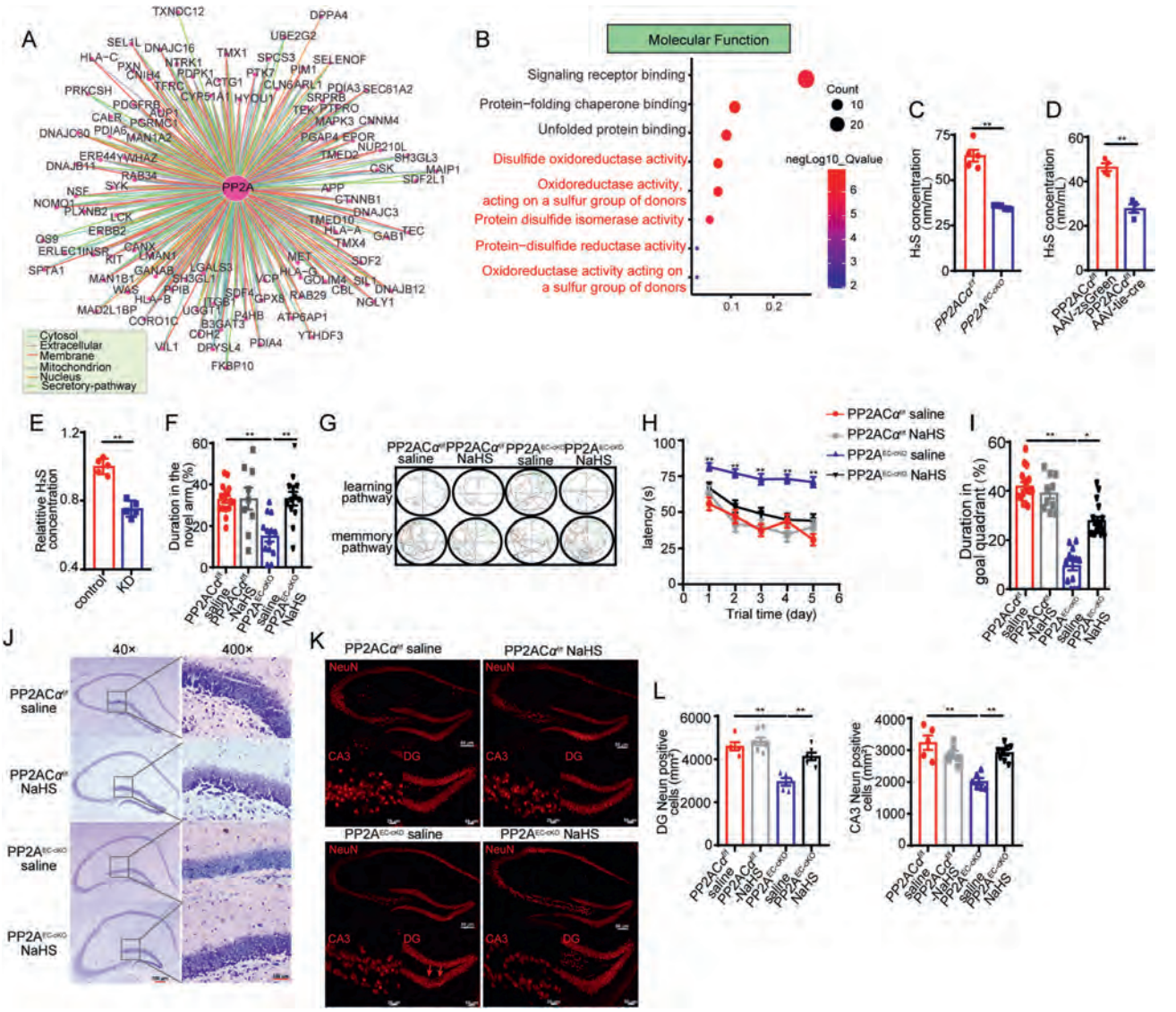

Figure 4 Endothelial PP2A deficiency resulted in a reduction of H_2S production in mice. (A, B) Bioinformation analysis for the interaction between PP2A and hydrogen sulfide. (C−E) Measurement of H_2S concentration. (C) PP2ACα$^{f/f}$ and PP2A$^{EC\text{-}cKO}$ PBMECs, (n = 5), (D) PP2ACα$^{f/f}$ PBMECs infected with AAV-Tie-cre (n = 4), (E) bEnd.3 cells were transfected with *Ppp2ca* shRNA, (n = 5). (F−I) Cognition was evaluated by Y-maze test (F) and Morris water maze test (G−I) at 2 days after termination of NaHS administration. (G) The typical swim path of PP2ACα$^{f/f}$-saline, PP2ACα$^{f/f}$-NaHS, PP2A$^{EC\text{-}cKO}$-saline, PP2A$^{EC\text{-}cKO}$-NaHS mice. (H) Latency to reach the hidden platform during the acquisition trial. (I) Percentage occupancy in the goal quadrant in the probe trial, (n = 9−14). (J) Nissl staining for neurodegeneration in the hippocampus of PP2ACα$^{f/f}$-saline, PP2ACα$^{f/f}$-NaHS, PP2A$^{EC\text{-}cKO}$-saline, PP2A$^{EC\text{-}cKO}$-NaHS mice (n = 5). Scale bar, 100 μm. (K, L) Representative confocal image (K) and quantification (L) of NeuN + neurons (red) in the CA3 and DG hippocampal subfield of PP2ACα$^{f/f}$-saline, PP2ACα$^{f/f}$-NaHS, PP2A$^{EC\text{-}cKO}$-saline, PP2A$^{EC\text{-}cKO}$-NaHS mice at 7 days after termination of NaHS administration (n = 5∼7). Scale bar, 20 or 50 μm. Data are expressed mean ± SEM, $^*P < 0.05$, $^{**}P < 0.01$.

Information Fig. S7A−S7G) and CBS (Fig. S7H−S7N). To confirm the interaction between MPST and PP2A, AAV9-Tie-*Mpst* and AAV-BR1-*Tie*1.EGFP.2A-m*Mpst* (or BR1-MPST) were used to overexpress MPST in brain ECs. A remarkable increase in MPST expression (Fig. 5H, Supporting Information Figs. S6J and S6K, S8A−S8D) and H_2S production (Fig. 5I) was observed in both the brain vasculature and PBMECs of PP2A$^{EC\text{-}cKO}$ mice three weeks after AAV-MPST injection. Interestingly, MPST overexpression in ECs significantly ameliorated the cognitive impairment in PP2A$^{EC\text{-}cKO}$ mice. This was evidenced by an increased discrimination index in the NOR tests (Fig. S8E and S8F), an increase in preference for the novel arm in the Y-maze (Fig. 5J and Fig. S8G), and Morris water maze trials (Fig. 5K−M). Furthermore, the restoration of MPST expression in brain ECs led to a significant increase in the number of NeuN^{+}-positive cells (Fig. 5N and O, Fig. S8H and S8I) in PP2A$^{EC\text{-}cKO}$ mice. Taken together, these results indicate that H_2S reduction-mediated neuronal dysfunction in PP2A$^{EC\text{-}cKO}$ mice is related to the suppression of endothelial MPST expression.

3.6. Endothelial PP2A deficiency promotes calpain2-mediated degradation of MPST

The quantitative RT-PCR analysis revealed that the inactivation of PP2A did not influence the level of *Mpst* transcript in PBMECs and bEnd.3 cells (Fig. 6A and B), indicating that PP2A inactivation reduces MPST expression through post-translational proteolytic mechanisms. We investigated the impact of the autophagy−lysosomal pathway and ubiquitin−proteasome system on MPST degradation. The autophagy−lysosomal pathway

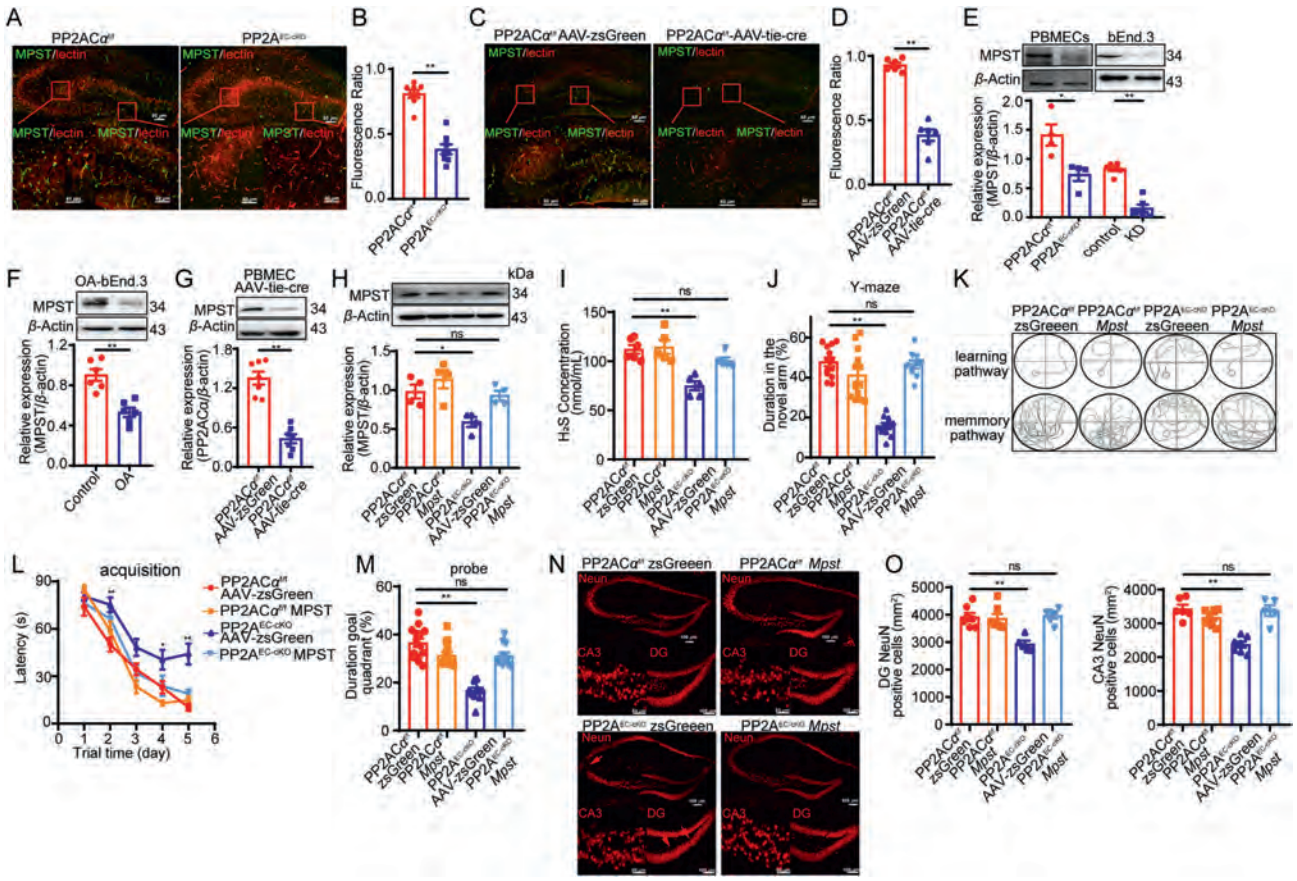

Figure 5 Endothelial PP2A deficiency suppressed MPST expression in mice. (A, B) Representative confocal images (A) and quantification (B) of MPST in hippocampal endothelium of PP2AC$\alpha^{f/f}$ and PP2A$^{EC\text{-}cKO}$ mice. MPST (green), Lectin (red) (n = 7−8). Scale bar, 50 μm. (C, D) Representative confocal images (C) and quantification (D) of MPST in hippocampal endothelium of PP2AC$\alpha^{f/f}$-zsGreen and PP2AC$\alpha^{f/f}$-AAV-Tie-cre mice (n = 6). MPST (green), Lectin (red). Scale bar = 50 μm. (E) Immunoblots of MPST proteins level in PBMECs and bEnd.3 cells (n = 4 for PBMECs; n = 5 for bEnd.3 cells). (F) Immunoblots of MPST proteins level in bEnd.3 cells. bEnd.3 cells were treated with 100 nmol/L okadaic acid (OA) to inhibit PP2A activity (n = 6). (G) Immunoblots of MPST proteins level in PBMECs lysates isolated from PP2AC$\alpha^{f/f}$ mice infected with AAV-zsGreen or AAV-Tie-cre (n = 7). (H) Immunoblots of MPST proteins level in PBMECs lysates isolated from PP2AC$\alpha^{f/f}$ and PP2A$^{EC\text{-}cKO}$ mice infected with AAV-zsGreen or AAV-Tie- *Mpst* (n = 4). (I) H_2S concentration in PBMECs lysates isolated from PP2AC$\alpha^{f/f}$ and PP2A$^{EC\text{-}cKO}$ mice infected with AAV-zsGreen or AAV-Tie-*Mpst* (n = 5−6). (J−M) Cognition was evaluated by Y-maze test (J) and Morris water maze test (K−M) at 3 weeks after AAV-Tie- *Mpst* injection. (K) The typical swim path of PP2AC$\alpha^{f/f}$-zsGreen, PP2AC$\alpha^{f/f}$-*Mpst*, PP2A$^{EC\text{-}cKO}$-zsGreen, PP2A$^{EC\text{-}cKO}$-*Mpst* mice. (L) Latency to reach the hidden platform during the acquisition trial. (M) Percentage occupancy in the goal quadrant in the probe trial (n = 10−13). (N, O) Representative confocal image (N) and quantification (O) of NeuN^{+} neurons (red) in the CA3 and DG hippocampal subfield of PP2AC$\alpha^{f/f}$-zsGreen, PP2AC$\alpha^{f/f}$-*Mpst*, PP2A$^{EC\text{-}cKO}$-zsGreen, PP2A$^{EC\text{-}cKO}$-*Mpst* (n = 5−7). Scale bar, 50 μm. Data are expressed as mean ± SEM, $^{*}P < 0.05$, $^{**}P < 0.01$.

was blocked by bafilomycin A; however, bafilomycin A did not impede MPST degradation induced by PP2A inactivation (Supporting Information Fig. S9A−S9C). By contrast, PP2A inactivation moderately attenuated autophagic activity (Fig. S9D and S9E), suggesting that MPST degradation is unrelated to autophagy. In addition, the application of MG132 to inhibit the ubiquitin-proteasome system in PBMECs did not effectively prevent MPST degradation (Fig. S9F−S9H). The involvement of PP2A in the regulation of the calpain system has been demonstrated in previous studies[30]. Calpains are calcium-regulated cytoplasmic cysteine proteases involved in the intracellular processing of proteins[31]. Interestingly, both the mRNA expression and protein levels of calpain2 and calpain1 were significantly upregulated in PP2A-deficient PBMECs (Fig. 6C−F). As depicted in Fig. 6G and H, the deficiency of PP2A induces a robust influx of calcium ions and an increase in the phosphorylation of calpain2 (Fig. 6I), suggesting that PP2A deficiency enhances the activity of calpain2. However, PP2A deficiency did not result in an increase in calpain1 phosphorylation (Fig. S9I). Furthermore, the results of the co-immunoprecipitation experiments demonstrated that PP2A inactivation led to increased binding between calpain2 and MPST (Fig. 6J and K). Importantly, administration of the calpain inhibitor PD150606 effectively reversed the reduction in MPST levels and blocked the increase in calpain2 induced by PP2A inactivation (Fig. 6L−N). Therefore, these findings suggest that PP2A inactivation results in an upregulation of both the expression and activity of calpain2, subsequently enhancing the interaction between calpain2 and MPST to induce MPST degradation, ultimately contributing to a decrease in endothelial H_2S production.

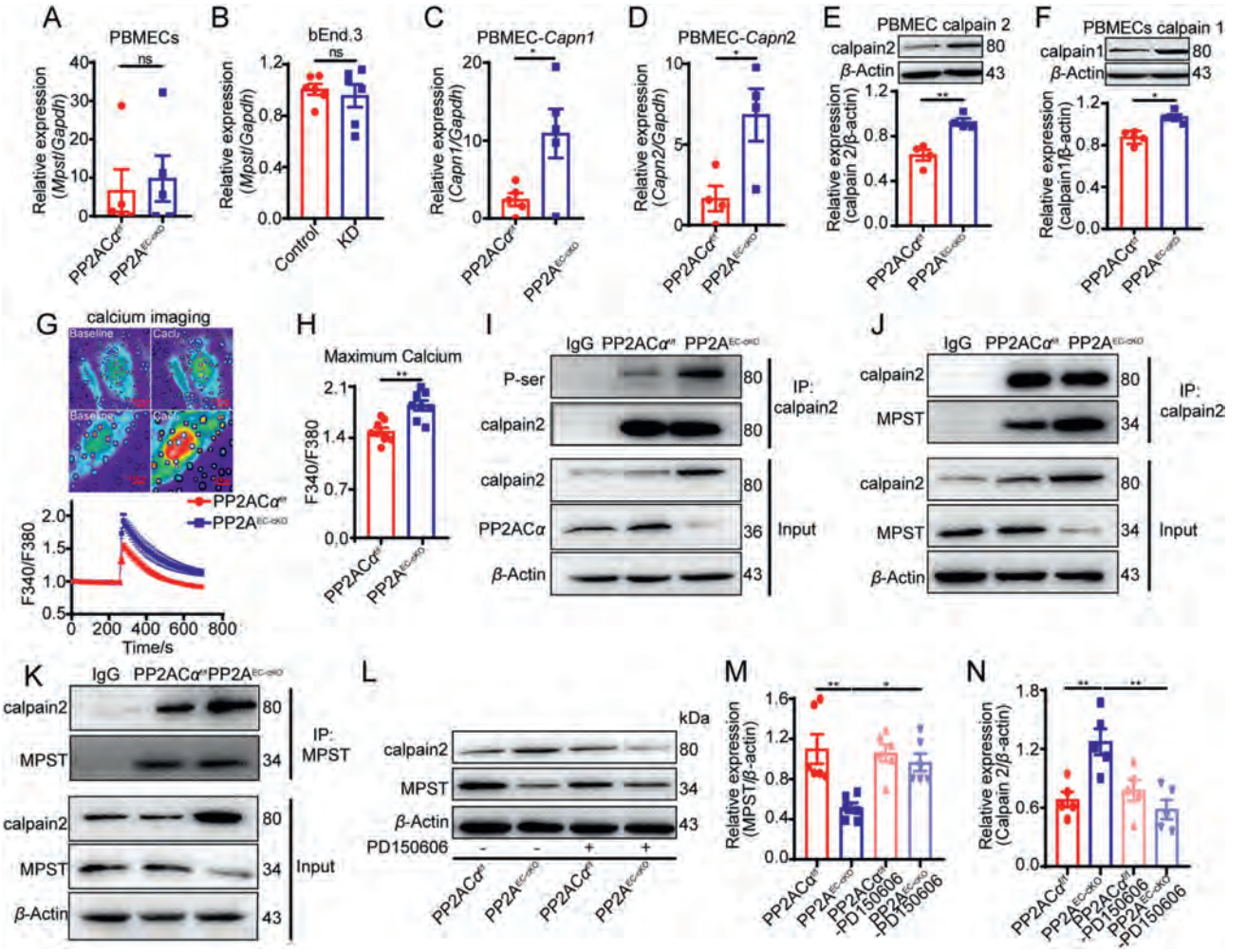

Figure 6 Endothelial PP2A deficiency promotes calpain2-mediated degradation of MPST. (A, B) Relative mRNA levels of MPST in PBMECs isolated from PP2AC$\alpha^{f/f}$ or PP2A$^{EC\text{-}cKO}$ mice ($n = 4$) (A) and bEnd.3 cells ($n = 6$) (B). (C, D) Relative mRNA levels of *Capn1* (C) and *Capn2* (D) in PBMECs lysates isolated from PP2AC$\alpha^{f/f}$ or PP2A$^{EC\text{-}cKO}$ mice ($n = 4$−5). (E, F) Immunoblots of calpain 2 (E) and calpain1 (F) proteins level in PBMECs lysates isolated from PP2AC$\alpha^{f/f}$ or PP2A$^{EC\text{-}cKO}$ mice ($n = 4$−5). (G) Representative line-scan images of Ca^{2+} sparks and time-dependent profiles of global Ca^{2+} influx induced by application of 0.3 mol/L $CaCl_2$ for PP2AC$\alpha^{f/f}$ and PP2A$^{EC\text{-}cKO}$ PBMECs. (H) Maximum amplitude of $CaCl_2$ induced Ca^{2+} transients. (I) Immunoblot analysis of calpain2 phosphorylation level in PP2AC$\alpha^{f/f}$ and PP2A$^{EC\text{-}cKO}$ PBMECs using phospho-serine antibody. (J) Immunoblot analysis of calpain2 and MPST proteins in PBMECs lysates immunoprecipitated with control IgG or anti-calpain2 antibody. (K) Immunoblot analysis of calpain2 and MPST proteins in PBMECs lysates immunoprecipitated with control IgG or anti-MPST antibody. (L−N) Immunoblots of calpain2 and MPST in PP2AC$\alpha^{f/f}$ and PP2A$^{EC\text{-}cKO}$ PBMECs. PBMECs were treated with vehicle or 40 μmol/L PD150606 for 12 h. Data are expressed as mean ± SEM, $^*P < 0.05$, $^{**}P < 0.01$.

3.7. *PP2A activator restores endothelial MPST expression and ischemic neuron dysfunction*

Based on these mechanistic studies, we investigated the potential application of PP2A activators in the treatment of ischemic cerebrovascular disease. C57BL/6J mice were subjected to cerebral ischemia *via* the LCA and treated with the PP2A activator FTY720 (2 mg/kg/day) or saline. Administration of FTY720 significantly enhanced the expression of endothelial MPST (Fig. 7A and B) and increased H_2S production (Fig. 7C) in ligated mice compared with observations in those treated with saline. Moreover, FTY720 attenuated ligation-induced cognitive deficits by reducing the latencies of ligated mice to find the hidden platform, increasing their exploration time in the goal quadrant during probe trials in the Morris water maze test, and increasing their preference for the novel arm in the Y-maze (Fig. 7D−G). In addition, ligation reduced the number of $NeuN^+$ positive cells, which was restored by FTY720 treatment (Fig. 7H and I). These results suggest that FTY720 impedes ischemia-induced neuronal dysfunction by promoting MPST-mediated H_2S production in the brain vascular endothelium.

3.8. *3MP restores endothelial MPST-dependent H_2S production and ischemic neuron dysfunction*

The substrate of MPST is 3MP, which reacts with MPST to generate H_2S *via* the formation of a persulfide intermediate. A previous study has revealed that 3MP promotes MPST-mediated H_2S production[32]. Therefore, we investigated whether 3MP could attenuate ischemic cerebrovascular dysfunction. C57BL/6J mice were also subjected to cerebral ischemia *via* the LCA and treated with 3MP sodium (1 mg/kg/day) or saline *via* intraperitoneal injection. 3MP sodium remarkably reversed the LCA-induced reduction in H_2S production compared with that in ligated mice treated with saline (Fig. 8A). We also found that 3MP sodium significantly enhanced MPST expression in brain microvascular endothelium (Fig. 8B and C) without altering PP2Acα (Fig. 8D and E). Moreover, 3MP sodium attenuated the ligation-

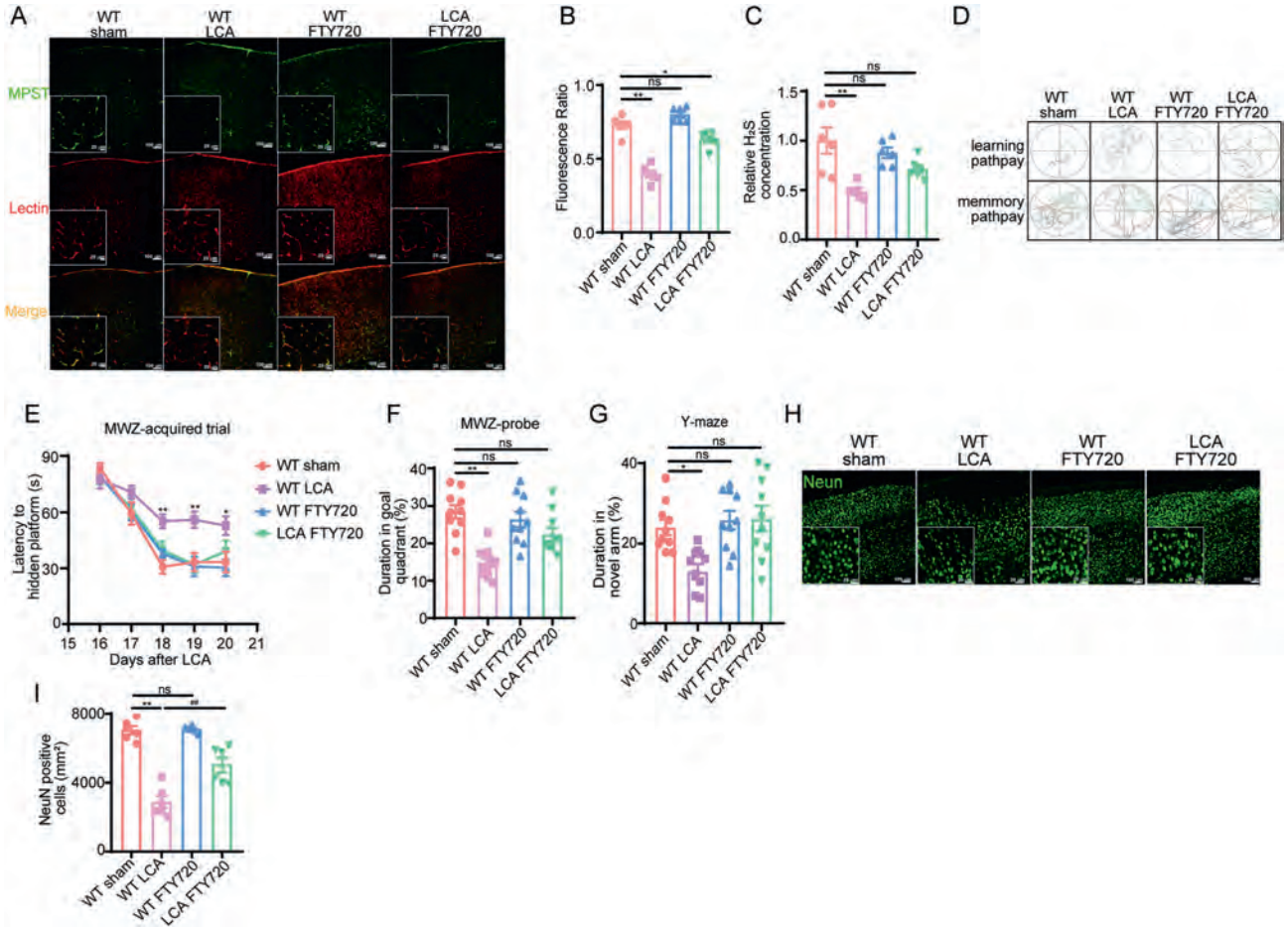

Figure 7 PP2A activator FTY720 restores ischemic neuron dysfunction and endothelial MPST expression. (A, B) Representative confocal image (A) and quantification (B) of MPST expression in brain endothelium. MPST (Green), $lectin^+$ (red). Scale bar, 20 μm. (C) Measurement of H_2S concentration after FTY720 treatment. (D−G) Cognition was evaluated by Morris water maze test (D−F) and Y-maze test (G) at 2 weeks after FTY720 treatment. (D) The typical swim path of WT or LCA mice treated with either vehicle (0.4% dimethyl sulfoxide in PBS) or FTY720 (2 mg/kg) by daily gavage. (E) Latency to reach the hidden platform during the acquisition trial. (F) Percentage occupancy in the goal quadrant in the probe trial. (G) Percentage time spent in the novel arm ($n = 10$−11). (H, I) Representative confocal image (H) and quantification (I) of $NeuN^+$ neurons in the brain ($n = 6$). Data are expressed as mean ± SEM, $^*P < 0.05$.

induced cognitive deficits, including increased time spent exploring novel objects in the NOR test (Fig. 8F and G) and the novel arm of the Y-maze (Fig. 8H). In addition, 3MP sodium significantly increased the number of $NeuN^+$ positive cells after LCA (Fig. 8I and J). These findings suggest that 3MP sodium effectively mitigated ischemia-induced neuronal dysfunction *via* an MPST/H_2S-dependent mechanism.

4. Discussion

PP2A is ubiquitously expressed in all cell types. It is widely recognized that in neurons of the brain, PP2A plays a protective role in cognitive function by inhibiting the hyperphosphorylation of α-synuclein and tau[33,34]. However, the role of endothelial PP2A in the brain remains unclear. Our study reveals a fundamental mechanism through which cerebral endothelial PP2A regulates MPST-mediated H_2S production and mitigates neuronal loss and hippocampal LTP deficits, thereby ameliorating cognitive dysfunction.

We observed a significant decrease in the α isoform catalytic subunit of PP2A (PP2ACα) within the vascular endothelium following cerebral ischemia. This finding is consistent with a previous study that reported chronic brain hypoperfusion-induced inactivation of PP2A through increased phosphorylation and demethylation of PP2AC[35]. Mice with congenital and acquired endothelial PP2A inactivation exhibit pronounced cognitive impairment, neuronal loss, and LTP deficits. Moreover, ischemia exacerbates cognitive dysfunction in $PP2A^{EC\text{-}cKO}$ mice. However, the restoration of PP2A activity in cerebral ECs significantly ameliorated neuronal dysfunction (Figs. 1−3 and Figs. S3 and S4). RNA sequencing of PBMECs in mononuclear cells revealed that endothelial PP2A plays a pivotal role in neurodegenerative diseases. Accumulating evidence suggests that abnormal communication between ECs and neurons is the key mechanism underlying cognitive dysfunction. Recent studies have demonstrated the importance of brain endothelial signaling pathways, such as PTEN−Akt−lactate and semaphorin 3G, in regulating adult hippocampal neurogenesis, synaptic plasticity, and proper positioning of neurons for effective communication in the NVU[36-39]. Our findings further support the essential role of endothelial signal transduction in the maintenance of normal neuronal function. *Ppp2cα* encodes the α isoform catalytic subunit of PP2A (PP2ACα), which is essential for maintaining PP2A activity; knockout of *Ppp2cα* leads to PP2A inactivation[40]. A study demonstrated an association between mutations in *PP2ACα* and intellectual disability and behavioral problems[41], consistent with the neuronal phenotype

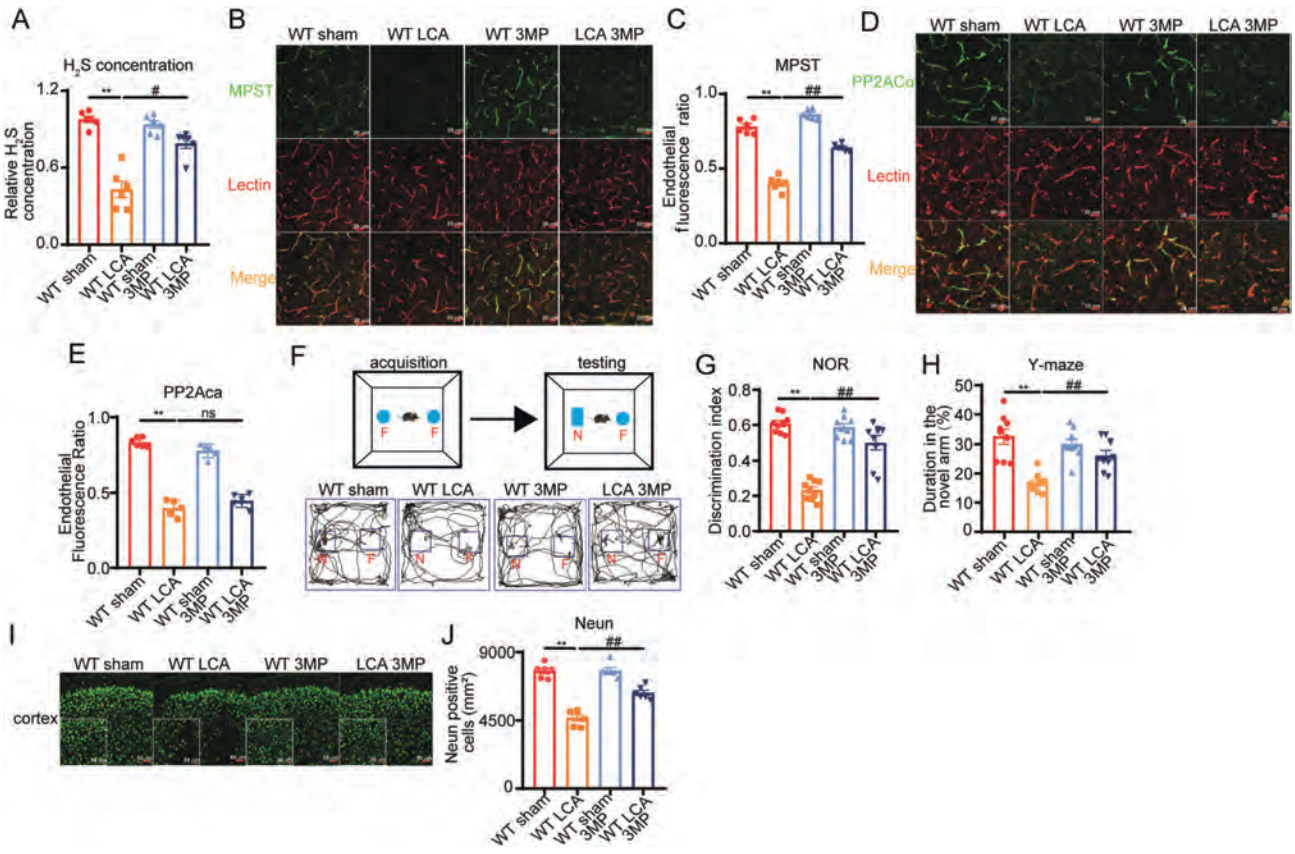

Figure 8 3MP sodium restores ischemic neuron dysfunction and endothelial MPST expression. (A) Measurement of H_2S concentration after 3MP sodium treatment. (B, C) Representative confocal image (B) and quantification (C) of MPST expression in brain endothelium. MPST (Green), $lectin^+$ (red). Scale bar, 20 μm. (D, E) Representative confocal image (D) and quantification (E) of PP2ACα expression in brain endothelium. PP2ACα (Green), $lectin^+$ (red). Scale bar, 20 μm. (F−H) Cognition was evaluated by Novel object recognition (F−G) and Y-maze test (H) at 12 days after 3MP sodium treatment. (F) The typical path of WT or LCA mice treated with either vehicle (0.4% dimethyl sulfoxide in PBS) or 3MP sodium (1 mg/kg) by daily i.p. (G) Discrimination index toward a novel object. (H) Percentage time spent in the novel arm ($n = 9$). (I, J) Representative confocal image (I) and quantification (J) of $NeuN^+$ neurons in the brain ($n = 6$). Data are expressed mean ± SEM, $^*P < 0.05$, $^{**}P < 0.01$.

observed in PP2A$^{EC\text{-}cKO}$ mice in this study. Furthermore, hippocampal neurons are known to exhibit early dysfunction in various diseases, such as AD and vascular dementia[42,43]. This observation might explain the predominant manifestation of hippocampal neuronal dysfunction in the initial phenotype. Subsequent investigations revealed that endothelial PP2A deficiency led to widespread neuronal dysfunction in the brain.

Brain ECs play a crucial role in regulating the integrity and continuous supply of CBF. To investigate the neuroprotective function of endothelial PP2A, we evaluated both BBB permeability and CBF. Interestingly, previous studies conducted by Le Guelte et al.[44] demonstrated that inhibition of endothelial PP2A results in increased permeability of brain ECs. However, our findings challenge the notion that endothelial PP2A deficiency compromises BBB integrity (Fig. S5A and S5B), suggesting potential variations in the impact of PP2A inactivation on different tight junctions. PP2A deficiency inhibits the dephosphorylation of occludin at the serine and threonine residues, leading to reduced endothelial permeability. Furthermore, our data indicated a significant upregulation of ZO-1 expression and downregulation of VE-cadherin upon PP2A inactivation (Fig. S5C). In addition, we observed no discernible effects on CBF following PP2A inactivation. Additional PP2A-regulated factors in ECs may modulate neuronal function. A previous study identified the secretion of EC-derived factors responsible for maintaining the self-renewal and neurogenic potential of the central nervous system[45]. The influence of PP2A on gas transmitters was suggested by its rapid diffusion characteristics. Recent studies have demonstrated neuroprotective effects of endothelium-derived H_2S[3]. Additionally, numerous studies extensively document the neuroprotective effects of H_2S, such as its ability to hinder the progression of PD and AD by inducing sulfhydration of Parkin and glycogen synthase kinase 3β[46-48]. Moreover, evidence strongly suggests that there is a significant decrease in H_2S levels during the progression of neurodegenerative diseases[49-51]. Furthermore, owing to its highly lipophilic characteristics, H_2S can readily permeate the cellular plasma membrane[49]. In our study, bioinformatics analysis revealed a strong interaction between H_2S catabolism and PP2A. Additionally, primary ECs deficient in PP2A showed a substantial decrease in H_2S levels (Fig. 4A−E). Moreover, the protective effect of exogenous H_2S in PP2A$^{EC\text{-}cKO}$ mice provided further evidence of the potential interaction between PP2A and H_2S (Fig. 4F and G). H_2S is generated endogenously from L-cysteine and catalyzed by CBS, CSE, and MPST[52]. Our findings revealed that PP2A deficiency contributed to a dramatic decrease in endothelial MPST without altering the expression of CBS or CSE (Fig. S7). Moreover, we found that cerebral MPST was mainly expressed in the vasculature system (Fig. S3I and S3J). Kuo et al.[53] confirmed that MPST is responsible for generating H_2S, which plays a crucial role in regulating coronary vasorelaxation. This finding highlights the significance of vascular MPST in H_2S production and distinguishes it from CSE. We further confirmed that overexpression of MPST in brain ECs significantly ameliorated neuronal impairment in PP2A$^{EC\text{-}cKO}$ mice (Fig. 4 and Fig. S8). In line with previous studies, MPST is of paramount importance in generating H_2S to maintain cerebral homeostasis[54,55]. Future studies should investigate the molecular mechanisms underlying endothelial H_2S reduction-induced neuronal functional impairment in PP2A$^{EC\text{-}cKO}$ mice. Chen et al.[56] have demonstrated that endothelial H_2S protects against neuronal dysfunction by inhibiting the RhoA−ROCK pathway in hippocampal neurons.

Our data show that endothelial PP2A deficiency did not affect MPST mRNA levels, suggesting posttranslational degradation of MPST. Previous studies have shown that PP2A promotes autophagy by inhibiting the mTOR/AKT pathway[57]. The expression of the MPST protein in PP2A deficient cells remained unchanged when the autophagy−lysosomal pathway and the ubiquitination system were inhibited (Fig. S9). It has been previously reported that PP2A dephosphorylates μ-calpain and m-calpain[30]. Calpain is a widely distributed calcium-sensitive protease. Surprisingly, our data suggest that calpain2 is involved in the endothelial PP2A/MPST signaling pathway, which regulates H_2S production in brain ECs (Fig. 6). Dysregulation of calpain activity may contribute to ischemic brain injury, AD, multiple sclerosis, and PD[58]. The activity of calpain2 is intricately associated with an intracellular calcium concentration[59]. The deficiency of PP2A leads to an increase in calcium influx, thereby activating calpain2 and subsequently promoting MPST degradation. Consistent with previous findings, PP2A downregulated L-type calcium channels, resulting in enhanced calcium influx[60]. Furthermore, our findings indicate that a deficiency in PP2A results in the upregulation of calpain2 phosphorylation and facilitates the direct interaction between calpain2 and MPST. These observations are consistent with those of a previous study that demonstrated that the phosphorylation of calpain2 contributes to its enhanced enzymatic activity[61]. Inhibition of calpain2 activity was found to hinder the degradation of MPST induced by PP2A inactivation, as revealed by our data.

Based on these mechanistic studies, we searched for drugs targeting the PP2A/MPST signaling pathway to treat cerebral ischemia. FTY720 is an activator of PP2A, which exhibits neuroprotective effects by increasing spine density[62]. Consistent with this finding, our data show that FTY720 attenuated ischemia-induced injury by targeting the brain endothelial MPST/H_2S pathway (Fig. 7). Additionally, the neuroprotective effects of 3MP sodium were investigated in PP2A$^{EC\text{-}cKO}$ mice by promoting MPST-dependent H_2S production, which has been shown to protect ECs[32]. The results of our study further supported the effectiveness of 3MP sodium in reducing neuronal dysfunction in PP2A$^{EC\text{-}cKO}$ mice (Fig. 8). These data strongly indicate that MPST is a promising candidate for the treatment of ischemic cerebrovascular diseases.

This study clarified the neuroprotective roles of cerebral endothelial MPST and PP2A. We found that PP2A deficiency in brain microvascular ECs induces calpain2-dependent degradation of MPST, followed by a reduction in H_2S production, subsequently contributing to neuronal dysfunction.

5. Conclusions

We demonstrated a novel mechanism involved in the regulation of crosstalk between brain ECs and neurons. The graphic abstract illustrates that the knockout of cerebral endothelial PP2ACα leads to PP2A inactivation, which subsequently enhances both the expression and activity of calpain2 through increased calcium influx and phosphorylation. Additionally, PP2A deficiency promotes direct binding between calpain2 and MPST, resulting in MPST degradation and reduced production of H_2S. Consequently, this disruption impairs the normal communication between cerebral ECs and neurons, leading to cognitive dysfunction and neuronal loss. Our study highlights the potential therapeutic targets of endothelial MPST for cardiovascular disease therapy.

Acknowledgments

This work was supported by the National Natural Science Foundation of China (Grant numbers 82274130), Key Program of National Natural Science Foundation of China (Grant numbers 81930113), National TCM Inheritance and Innovation Team Project Foundation of China (Grant numbers ZYYCXTD-C-202201), Key Laboratory of Heart and Spleen Related Diseases and Prescriptions Foundation of Guangdong Province (Grant number 2022B1212010012, China), the Guangzhou Basic and Applied Research Foundation (Grant number SL2023A04J01903, China) and the Major Program of Science and Technology Foundation of Guangzhou (Grant number 202103000044, China).

Author contributions

Li Zhu: Writing − review & editing, Writing − original draft, Visualization, Validation, Resources, Project administration, Methodology, Investigation, Formal analysis, Data curation. Yi Huang: Methodology, Investigation, Formal analysis. Jing Jin: Supervision, Methodology, Data curation, Conceptualization. Rongjun Zou: Visualization, Software, Methodology. Rui Zuo: Supervision, Investigation, Data curation. Yong Luo: Investigation. Ziqing Song: Investigation. Linfeng Dai: Investigation. Minyi Zhang: Investigation. Qiuhe Chen: Investigation. Yunting Wang: Investigation. Wei Wang: Funding acquisition. Rongrong He: Funding acquisition, Conceptualization. Yang Chen: Supervision, Funding acquisition, Formal analysis, Data curation, Conceptualization.

Conflicts of interest

The authors declare no conflicts of interest.

Appendix A. Supporting information

Supporting information to this article can be found online at https://doi.org/10.1016/j.apsb.2024.11.015.

References

1. Schaeffer S, Iadecola C. Revisiting the neurovascular unit. *Nat Neurosci* 2021;**24**:1198−209.
2. Sweeney MD, Zhao Z, Montagne A, Nelson AR, Zlokovic BV. Blood−brain barrier: from physiology to disease and back. *Physiol Rev* 2019;**99**:21−78.
3. Wen JY, Zhang J, Chen S, Chen Y, Zhang Y, Ma ZY, et al. Endothelium-derived hydrogen sulfide acts as a hyperpolarizing factor and exerts neuroprotective effects *via* activation of large-conductance Ca^{2+}-activated K^+ channels. *Br J Pharmacol* 2021;**178**:4155−75.
4. Nagahara N. Multiple role of 3-mercaptopyruvate sulfurtransferase: antioxidative function, H_2S and polysulfide production and possible SO*x* production. *Br J Pharmacol* 2018;**175**:577−89.
5. Rao SP, Xie W, Kwon YIC, Juckel N, Xie JS, Dronamraju VR, et al. Sulfanegen stimulates 3-mercaptopyruvate sulfurtransferase activity and ameliorates Alzheimer's disease pathology and oxidative stress *in vivo*. *Redox Biol* 2022;**57**:102484.
6. Yang BB, Zhao WJ, Yin CS, Bai Y, Wang SH, Xing GW, et al. Acute acrylonitrile exposure inhibits endogenous H2S biosynthesis in rat brain and liver: the role of CBS/3-MPST−H_2S pathway in its astrocytic toxicity. *Toxicology* 2021;**451**:152685.
7. Zhang F, Chen S, Wen JY, Chen ZW. 3-Mercaptopyruvate sulfurtransferase/hydrogen sulfide protects cerebral endothelial cells against oxygen−glucose deprivation/reoxygenation-induced injury *via* mitoprotection and inhibition of the RhoA/ROCK pathway. *Am J Physiol Cel Physiol* 2020;**319**:C720−33.
8. Huttlin EL, Jedrychowski MP, Elias JE, Goswami T, Rad R, Beausoleil SA, et al. A tissue-specific atlas of mouse protein phosphorylation and expression. *Cell* 2010;**143**:1174−89.
9. Lundby A, Secher A, Lage K, Nordsborg NB, Dmytriyev A, Lundby C, et al. Quantitative maps of protein phosphorylation sites across 14 different rat organs and tissues. *Nat Commun* 2012;**3**:876.
10. Yang CC, Li XL, Gao WB, Wang Q, Zhang L, Li YL, et al. Cornel iridoid glycoside inhibits tau hyperphosphorylation *via* regulating cross-talk between GSK-3 beta and PP2A signaling. *Front Pharmacol* 2018;**9**:682.
11. Perez-Revuelta BI, Hettich MM, Ciociaro A, Rotermund C, Kahle PJ, Krauss S, et al. Metformin lowers Ser-129 phosphorylated alpha-synuclein levels *via* mTOR-dependent protein phosphatase 2A activation. *Cell Death Dis* 2014;**5**:e1209.
12. Sen T, Saha P, Jiang T, Sen N. Sulfhydration of AKT triggers Tau-phosphorylation by activating glycogen synthase kinase 3 beta in Alzheimer's disease. *Proc Natl Acad Sci U S A* 2020;**117**:4418−27.
13. Zhang J, Cen L, Zhang XF, Tang CX, Chen YS, Zhang YW, et al. MPST deficiency promotes intestinal epithelial cell apoptosis and aggravates inflammatory bowel disease *via* AKT. *Redox Biol* 2022;**56**:102469.
14. Yu G, Wang LG, Han Y, He QY. clusterProfiler: an R package for comparing biological themes among gene clusters. *Omics* 2012;**16**:284−7.
15. Szklarczyk D, Gable AL, Nastou KC, Lyon D, Kirsch R, Pyysalo S, et al. The STRING database in 2021: customizable protein−protein networks, and functional characterization of user-uploaded gene/-measurement sets. *Nucleic Acids Res* 2021;**49**:D605-12.
16. von Mering C, Huynen M, Jaeggi D, Schmidt S, Bork P, Snel B. STRING: a database of predicted functional associations between proteins. *Nucleic Acids Res* 2003;**31**:258−61.
17. Shannon P, Markiel A, Ozier O, Baliga NS, Wang JT, Ramage D, et al. Cytoscape: a software environment for integrated models of biomolecular interaction networks. *Genome Res* 2003;**13**:2498−504.
18. Veres DV, Gyurkó DM, Thaler B, Szalay KZ, Fazekas D, Korcsmáros T, et al. ComPPI: a cellular compartment-specific database for protein−protein interaction network analysis. *Nucleic Acids Res* 2015;**43**:D485−93.
19. Auer F, Hammoud Z, Ishkin A, Pratt D, Ideker T, Kramer F. ndexr-an R package to interface with the network data exchange. *Bioinformatics* 2018;**34**:716−7.
20. Wang H, Hong LJ, Huang JY, Jiang Q, Tao RR, Tan C, et al. $P2RX_7$ sensitizes Mac-1/ICAM-1-dependent leukocyte-endothelial adhesion and promotes neurovascular injury during septic encephalopathy. *Cell Res* 2015;**25**:674−90.
21. Zheng LF, Yu M, Lin R, Wang YX, Zhuo Z, Cheng N, et al. Rhythmic light flicker rescues hippocampal low gamma and protects ischemic neurons by enhancing presynaptic plasticity. *Nat Commun* 2020;**11**:3012.
22. Nam D, Ni CW, Rezvan A, Suo J, Budzyn K, Llanos A, et al. Partial carotid ligation is a model of acutely induced disturbed flow, leading to rapid endothelial dysfunction and atherosclerosis. *Am J Physiol Heart Circ Physiol* 2009;**297**:H1535−43.
23. Kamat PK, Kalani A, Givvimani S, Sathnur PB, Tyagi SC, Tyagi N. Hydrogen sulfide attenuates neurodegeneration and neurovascular dysfunction induced by intracerebral-administered homocysteine in mice. *Neuroscience* 2013;**252**:302−19.
24. Yao S, Li L, Sun X, Hua J, Zhang K, Hao L, et al. FTY720 inhibits MPP^+-induced microglial activation by affecting NLRP3 inflammasome activation. *J Neuroimmune Pharmacol* 2019;**14**:478−92.
25. Coletta C, Módis K, Szczesny B, Brunyánszki A, Oláh G, Rios EC, et al. Regulation of vascular tone, angiogenesis and cellular bioenergetics by the 3-mercaptopyruvate sulfurtransferase/H_2S pathway: functional impairment by hyperglycemia and restoration by DL-α-lipoic acid. *Mol Med* 2015;**21**:1−14.

26. Sacharidou A, Chambliss KL, Ulrich V, Salmon JE, Shen YM, Herz J, et al. Antiphospholipid antibodies induce thrombosis by PP2A activation *via* apoER2−Dab2−SHC1 complex formation in endothelium. *Blood* 2018;**131**:2097−110.
27. Teo TH, Howland SW, Claser C, Gun SY, Poh CM, Lee WWL, et al. Co-infection with Chikungunya virus alters trafficking of pathogenic $CD8^+$ T cells into the brain and prevents *Plasmodium*-induced neuropathology. *EMBO Mol Med* 2018;**10**:121−38.
28. Dang R, Wang M, Li X, Wang H, Liu L, Wu Q, et al. Edaravone ameliorates depressive and anxiety-like behaviors *via* Sirt1/Nrf2/HO-1/Gpx4 pathway. *J Neuroinflammation* 2022;**19**:41.
29. Lian L, Wang Y, Draznin J, Eslin D, Abrams CSJB. The relative role of PLCβ and PI3Kγ in platelet activation. *Blood* 2005;**106**:110−7.
30. Xu L, Deng X. Suppression of cancer cell migration and invasion by protein phosphatase 2A through dephosphorylation of mu- and m-calpains. *J Biol Chem* 2006;**281**:35567−75.
31. Christodoulou N, Skourides PA. Cell-autonomous Ca^{2+} flashes elicit pulsed contractions of an apical actin network to drive apical constriction during neural tube closure. *Cell Rep* 2015;**13**:2189−202.
32. Govar AA, Töro G, Szaniszlo P, Pavlidou A, Bibli SI, Thanki K, et al. 3-Mercaptopyruvate sulfurtransferase supports endothelial cell angiogenesis and bioenergetics. *Br J Pharmacol* 2020;**177**:866−83.
33. Lee KW, Chen W, Junn E, Im JY, Grosso H, Sonsalla PK, et al. Enhanced phosphatase activity attenuates alpha-synucleinopathy in a mouse model. *J Neurosci* 2011;**31**:6963−71.
34. Shentu YP, Huo YD, Feng XL, Gilbert J, Zhang Q, Liuyang ZY, et al. CIP2A causes tau/APP phosphorylation, synaptopathy, and memory deficits in Alzheimer's disease. *Cel Rep* 2018;**24**:713−23.
35. Liu CD, Wang Q, Zong DK, Pei SC, Yan Y, Yan ML, et al. Knockdown of microRNA-195 contributes to protein phosphatase-2A inactivation in rats with chronic brain hypoperfusion. *Neurobiol Aging* 2016;**45**:76−87.
36. Wang J, Cui YX, Yu ZY, Wang WJ, Cheng X, Ji WL, et al. Brain endothelial cells maintain lactate homeostasis and control adult hippocampal neurogenesis. *Cell Stem Cell* 2019;**25**:754−67. e9.
37. Tan C, Lu NN, Wang CK, Chen DY, Sun NH, Lyu H, et al. Endothelium-derived semaphorin 3G regulates hippocampal synaptic structure and plasticity *via* peuropilin-2/plexinA4. *Neuron* 2019;**101**:920−37.
38. Segarra M, Aburto MR, Cop F, Llao-Cid C, Hartl R, Damm M, et al. Endothelial Dab1 signaling orchestrates neuro-glia-vessel communication in the central nervous system. *Science* 2018;**361**:eaao2861.
39. Han L, Jiang C. Evolution of blood−brain barrier in brain diseases and related systemic nanoscale brain-targeting drug delivery strategies. *Acta Pharm Sin B* 2021;**11**:2306−25.
40. Shi YG. Serine/threonine phosphatases: mechanism through structure. *Cell* 2009;**139**:468−84.
41. Reynhout S, Jansen S, Haesen D, van Belle S, de Munnik S, Bongers E, et al. *De novo* mutations affecting the catalytic Cα subunit of PP2A, PPP2CA, cause syndromic intellectual disability resembling other PP2A-related neurodevelopmental disorders. *Am J Hum Genet* 2019;**104**:139−56.
42. Coughlan G, Laczó J, Hort J, Minihane AM, Hornberger M. Spatial navigation deficits—overlooked cognitive marker for preclinical Alzheimer disease? *Nat Rev Neurol* 2018;**14**:496−506.
43. Shaw K, Bell L, Boyd K, Grijseels DM, Clarke D, Bonnar O, et al. Neurovascular coupling and oxygenation are decreased in hippocampus compared to neocortex because of microvascular differences. *Nat Commun* 2021;**12**:3190.
44. Le Guelte A, Galan-Moya EM, Dwyer J, Treps L, Kettler G, Hebda JK, et al. Semaphorin 3A elevates endothelial cell permeability through PP2A inactivation. *J Cel Sci* 2012;**125**:4137−46.
45. Shen Q, Goderie SK, Jin L, Karanth N, Sun Y, Abramova N, et al. Endothelial cells stimulate self-renewal and expand neurogenesis of neural stem cells. *Sci (New York, NY)* 2004;**304**:1338−40.
46. Vandiver MS, Paul BD, Xu RS, Karuppagounder S, Rao F, Snowman AM, et al. Sulfhydration mediates neuroprotective actions of parkin. *Nat Commun* 2013;**4**:1626.
47. Giovinazzo D, Bursac B, Sbodio JI, Nalluru S, Vignane T, Snowman AM, et al. Hydrogen sulfide is neuroprotective in Alzheimer's disease by sulfhydrating GSK3 beta and inhibiting Tau hyperphosphorylation. *Proc Natl Acad Sci U S A* 2021;**118**:e2017225118.
48. Wang P, Wang F, Ni L, Wu P, Chen J. Targeting redox-altered plasticity to reactivate synaptic function: a novel therapeutic strategy for cognitive disorder. *Acta Pharm Sin B* 2021;**11**:599−608.
49. Panthi S, Chung HJ, Jung J, Jeong NY. Physiological importance of hydrogen sulfide: emerging potent neuroprotector and neuromodulator. *Oxid Med Cel Longev* 2016;**2016**:9049782.
50. Paul BD, Sbodio JI, Xu RS, Vandiver MS, Cha JY, Snowman AM, et al. Cystathionine gamma-lyase deficiency mediates neurodegeneration in Huntington's disease. *Nature* 2014;**509**:96−100.
51. Sbodio JI, Snyder SH, Paul BD. Golgi stress response reprograms cysteine metabolism to confer cytoprotection in Huntington's disease. *Proc Natl Acad Sci U S A* 2018;**115**:780−5.
52. Donnarumma E, Trivedi RK, Lefer DJ. Protective actions of H_2S in acute myocardial infarction and heart failure. *Compr Physiol* 2017;**7**:583−602.
53. Kuo MM, Kim DH, Jandu S, Bergman Y, Tan S, Wang H, et al. MPST but not CSE is the primary regulator of hydrogen sulfide production and function in the coronary artery. *Am J Physiol Heart Circ Physiol* 2016;**310**:H71−9.
54. Shibuya N, Tanaka M, Yoshida M, Ogasawara Y, Togawa T, Ishii K, et al. 3-Mercaptopyruvate sulfurtransferase produces hydrogen sulfide and bound sulfane sulfur in the brain. *Antioxid Redox Signal* 2009;**11**:703−14.
55. Kimura Y, Toyofuku Y, Koike S, Shibuya N, Nagahara N, Lefer D, et al. Identification of H_2S_3 and H_2S produced by 3-mercaptopyruvate sulfurtransferase in the brain. *Sci Rep* 2015;**5**:14774.
56. Chen Y, Wen J, Chen Z. H_2S protects hippocampal neurons against hypoxia-reoxygenation injury by promoting RhoA phosphorylation at Ser188. *Cell Death Discov* 2021;**7**:132.
57. Lu S, Yao Y, Xu G, Zhou C, Zhang Y, Sun J, et al. CD24 regulates sorafenib resistance *via* activating autophagy in hepatocellular carcinoma. *Cel Death Dis* 2018;**9**:646.
58. McAleese KE, Walker L, Graham S, Moya ELJ, Johnson M, Erskine D, et al. Parietal white matter lesions in Alzheimer's disease are associated with cortical neurodegenerative pathology, but not with small vessel disease. *Acta Neuropathol* 2017;**134**:459−73.
59. Goll DE, Thompson VF, Li H, Wei W, Cong J. The calpain system. *Physiol Rev* 2003;**83**:731−801.
60. Chen XW, Piancentino V, Furukawa S, Goldman B, Margulies KB, Houser SR. L-type Ca^{2+} channel density and regulation are altered in failing human ventricular myocytes and recover after support with mechanical assist devices. *Circ Res* 2002;**91**:517−24.
61. Bugide S, David D, Nair A, Kannan N, Samanthapudi VSK, Prabhakar J, et al. Hematopoietic PBX-interacting protein (HPIP) is over expressed in breast infiltrative ductal carcinoma and regulates cell adhesion and migration through modulation of focal adhesion dynamics. *Oncogene* 2015;**34**:4601−12.
62. Liu X, Huai J, Endle H, Schlüter L, Fan W, Li Y, et al. PRG-1 regulates synaptic plasticity *via* intracellular PP2A/β1-integrin signaling. *Dev Cel* 2016;**38**:275−90.